AA Technical Memorandum ERL ARL-99

CHARACTERISTICS OF ULTRAVIOLET RADIATION IN THE HUMAN ERYTHEMA BAND MEASURED WITH A ROBERTSON-BERGER METER AND A DOUBLE MONOCHROMATOR

John J. DeLuisi
Joyce M. Harris

Air Resources Laboratories
Silver Spring, Maryland
March 1981

noaa NATIONAL OCEANIC AND ATMOSPHERIC ADMINISTRATION / Environmental Research Laboratories

NOAA Technical Memorandum ERL ARL-99

CHARACTERISTICS OF ULTRAVIOLET RADIATION IN THE HUMAN ERYTHEMA BAND MEASURED WITH A ROBERTSON-BERGER METER AND A DOUBLE MONOCHROMATOR

John J. DeLuisi
Joyce M. Harris

Geophysical Monitoring for Climatic Change
Boulder, Colorado

Air Resources Laboratories
Silver Spring, Maryland
March 1981

UNITED STATES DEPARTMENT OF COMMERCE
Malcolm Baldrige, Secretary

NATIONAL OCEANIC AND ATMOSPHERIC ADMINISTRATION
James P. Walsh, Acting Administrator

Environmental Research Laboratories
Joseph O. Fletcher, Acting Director

NOTICE

Mention of a commercial company or product does not constitute an endorsement by NOAA Environmental Research Laboratories. Use for publicity or advertising purposes of information from this publication concerning proprietary products or the tests of such products is not authorized.

CONTENTS

LIST OF SYMBOLS

Ω	Total ozone
λ	Wavelength in nanometers
I	Radiant intensity - power per unit solid angle per unit area per unit wavelength
F	Radiant flux - power per unit area per unit wavelength
F_o	Extraterrestrial solar flux
θ_o	Solar zenith angle
F_s	Directly transmitted solar flux
F_d	Diffusely transmitted hemispheric flux
F_t	Total hemispheric flux or direct plus diffuse hemispheric flux $F_t = F_s + F_d$
E_c	Radiant power for total hemispheric flux and integrated over a wavelength interval $\Delta\lambda$ corresponding to human erythema response
δ	Optical depth of aerosols
P	Atmospheric pressure where P_o = 1013.3 mb is standard sea level pressure
$K(\theta_o)$	Diffuser plate correction factor
$\varepsilon(\theta_o)$	Diffuser plate error function
$\Phi(\lambda)$	Band response function for human erythemal action spectrum or Robertson-Berger meter response
$\chi(\theta_o)$	Absolute radiant energy per sunburn unit
RB_c	Estimated absolute flux ($\mu W\ cm^{-1}$) in the RB meter bandpass using spectral flux observations
RB_m	RB meter measurements (counts per half-hour)
SU	Sunburn unit

CHARACTERISTICS OF ULTRAVIOLET RADIATION IN THE HUMAN ERYTHEMA BAND MEASURED WITH A ROBERTSON-BERGER METER AND A DOUBLE MONOCHROMATOR

John J. DeLuisi and Joyce M. Harris

ABSTRACT

In an in-depth analysis, data from a Robertson-Berger (RB) erythema flux meter were compared with concurrent measurements obtained with an ultraviolet spectroradiometer and with theoretically calculated uv fluxes. The absolute energy of one sunburn unit measured by the RB-meter was determined. It was found that at a solar zenith angle of 30° one sunburn unit (SU) is equivalent to 35 ± 4 mJ cm^{-2}, and at a solar zenith angle of 69° one SU is equivalent to 20 ± 2 mJ cm^{-2} (relative to a wavelength of 297 nm), where the rate of change is nonlinear. The difference is due to the RB-meter's imperfect simulation of the response of human skin to the incident uv solar spectrum. Moreover, the rate of growth of the deviation with increasing solar zenith angle was found to be 1.2% per degree between solar zenith angles 30° to 50° and 2.3% per degree between solar zenith angles 50° to 70°. These deviations of response with solar zenith angle were found to be consistent with reported RB-meter characteristics. Also given are examples of relative errors in RB-meter data due to latitude and seasonal variations in solar zenith angle.

1. INTRODUCTION

In its great and mysterious scheme of interactive bio-geophysical phenomena Nature has succeeded in protecting life as we now know it from harmful short-wave radiation by creating a thin but delicate screen of ozone. Yet this harmful radiation is responsible for creating part of the screen. In particular, radiation $\lambda \lesssim 250$ nm dissociates oxygen which in turn forms ozone. The ozone shield cuts off most of the uv radiation $\lambda \lesssim 290$ nm from reaching the Earth's surface, but the transmission of uv radiation rapidly increases with increasing wavelength until, beyond $\lambda \gtrsim 320$ nm, ozone has little effect. This relatively narrow wavelength region of the entire solar electromagnetic spectrum plays a rather paradoxical role in the ecology of the biosphere. Too much exposure to the uv radiation can cause harmful cell damage to the surfaces of many plants and animals in the oceans and on land; uv radiation also kills many kinds of microbes, some of which are harmful and some of which are beneficial to life. On the other hand, nature utilizes uv radiation to produce in plants and animals certain chemicals that are beneficial to their health. Thus, over the eons of Earth's biological habitation one would expect slow adjustments of genetic factors that are nearly in balance with the ultraviolet climatology of a particular epoch. The ultraviolet climatology will have changed in accordance with the evolution of the atmosphere.

Recently, through photochemical modeling efforts, there was recognized a potential threat to the ozone layer from anthropogenic pollution: global ozone could be reduced by 15%-40% in a few decades! Two examples of concern were the SST, and increasing concentrations of freons over the globe. In view of such a potentially rapid change, compared with changes on an evolutionary time scale, the important question that followed was, "Will there be serious consequences to the biosphere if uv radiation increases?" Sensitivity studies indicate that human skin cancer could be increased by 44% for a 16% decrease in total ozone. Although effects of drastic exposures of uv to biological specimens can be studied easily in the laboratory, a change in atmospheric ozone on the order of 10%-20%, which in turn may increase uv exposure by 20%-40%, is likely to produce biological changes at such a subtle rate that they cannot be detected by observing epidemiological changes in large populations in reasonable time. Moreover, by the time a change is observed, it may be too late to reverse it quickly because of the long residence time of released freons. Since human life is expected to exist indefinitely, it becomes practical to measure characteristics in uv radiation and correlate these with epidemiologic records of diseases that could be brought on by a change in exposure to uv radiation. Thus, a baseline will be established for future reference.

To establish a current baseline (or reference) set of uv data against which trends can be established, as well as to create an understanding of the variability of uv with time and the atmospheric variables that affect its transmission, simple, rugged uv sensors were placed at various sites to collect data continuously for several years (Machta et al., 1975, and Berger, 1976). The instrument selected for the task, the Robertson-Berger meter, was meant to simulate the human skin action spectrum (Berger, 1976). However, the instrument's bandpass is quite wide and does not perfectly simulate that of the human action spectrum. (At present, the action spectrum of human skin is not well defined because of the large variation in sunburning among humans.) Because of the extremely steep falloff of uv radiation toward shorter wavelengths in the bandpass region of the instrument, some deviation can be expected between the Robertson-Berger instrument's response and the response of an ideal instrument designed for the human skin action spectrum. This report describes the results of an experiment that was designed to measure uv radiation in the human action spectrum for comparison with Robertson-Berger meter measurements made side-by-side.

2. INSTRUMENTATION

The instrument used in this experiment was a Robertson-Berger meter (hereafter RB-meter) of the type now in operation in the EPA-NOAA network. A description of this instrument is given by Berger (1976). The spectral response of the RB-meter was intended to approximate the erythema action spectrum (Coblentz and Stair, 1934). The shapes of the wavelength response of the RB-meter and erythema action spectrum are indeed similar with the exception that the RB-meter curve is shifted towards longer wavelengths by about 10-15 nm from the erythema curve. Since the wavelength range of measurement is in the uv region of rapidly increasing attenuation with decreasing wavelength ($2<320$ nm), deviation of the instrument's response from the expected erythema is unavoidable.

The instrumentation for the spectral measurements consisted of two 0.25-meter Jerrell-Ash grating monochromators in tandem configuration. Slits were chosen to provide a nominal 0.8-nm bandpass. A solar blind photomultiplier was used for the detector. Output from the logarithmically amplified photomultiplier signal was fed to a chart recorder. The double monochromator (DM) gratings were coupled by a belt and pulley system, and were driven by a constant-speed motor at the rate of 12.5 nm min^{-1}. The fore-optical section of the DM consisted of a 90° periscope with a stainless steel mirror at the elbow. A horizontally oriented quartz diffuser plate was positioned on top of the periscope. This arrangement permitted the operation of the instrument on its normal base. By alternately exposing the diffuser to the total hemispheric sky radiation (which includes direct sunlight), and shading out the direct solar radiation, diffuse sky and direct Sun components can then be separated. Although only the total hemispheric flux is of interest in the present work, separation of the components is useful for checking the accuracy of the measurements and correcting for errors related to the angular response of the diffuser. Details of the DM system and its characteristics are given in Appendix A.

A flat-plate diffuser will almost invariably be in error with respect to a pure cosine response as the incident angle varies. Figure 1 shows the deviation of the quartz diffuser from an ideal cosine response. A correction for the direct solar radiation can be made simply by referring to the appropriate zenith angle in Figure 1 and then applying the corresponding correction to the measurement. For example, at a solar zenith angle of 50°, the measured direct radiation must be divided by 1.158.

Quartz diffuser cosine response deviations for diffuse hemispheric sky radiation appear to be complicated to correct. However, it turns out that a reasonable correction is rather simple to make. This is due to the fact that the uv diffuse sky intensity does not vary drastically with direction and that the diffuse hemispheric sky radiation is an integral quantity. At zenith angles of 0° and 90° the contribution to the integral is 0; at 45° the contribution is a maximum. The reason becomes obvious upon examination of integral given below. The hemispheric sky flux F_d is given by integrating diffuse sky intensities, I. Thus,

$$F_d\,(\lambda,\Omega,\theta_o) = \int_0^{2\pi}\int_0^{\pi/2} I(\theta,\Omega,\lambda)\,\cos\theta\,\sin\theta\,d\theta d\phi \quad ,$$

where λ stands for wavelength, Ω is total ozone, θ_o is the solar zenith angle and ϕ is azimuth. Note that the product $\cos\theta\,\sin\theta$ is 0 for $\theta=0$ or $\pi/2$.

If we introduce an error function $\varepsilon(\theta)$ for the diffuser plate we have

$$F_\varepsilon\,(\lambda,\Omega,\theta_o) = \int_0^{2\pi}\int_0^{\pi/2} I(\theta,\Omega,\lambda)\,\varepsilon(\theta)\,\cos\theta\,\sin\theta\,d\theta d\phi.$$

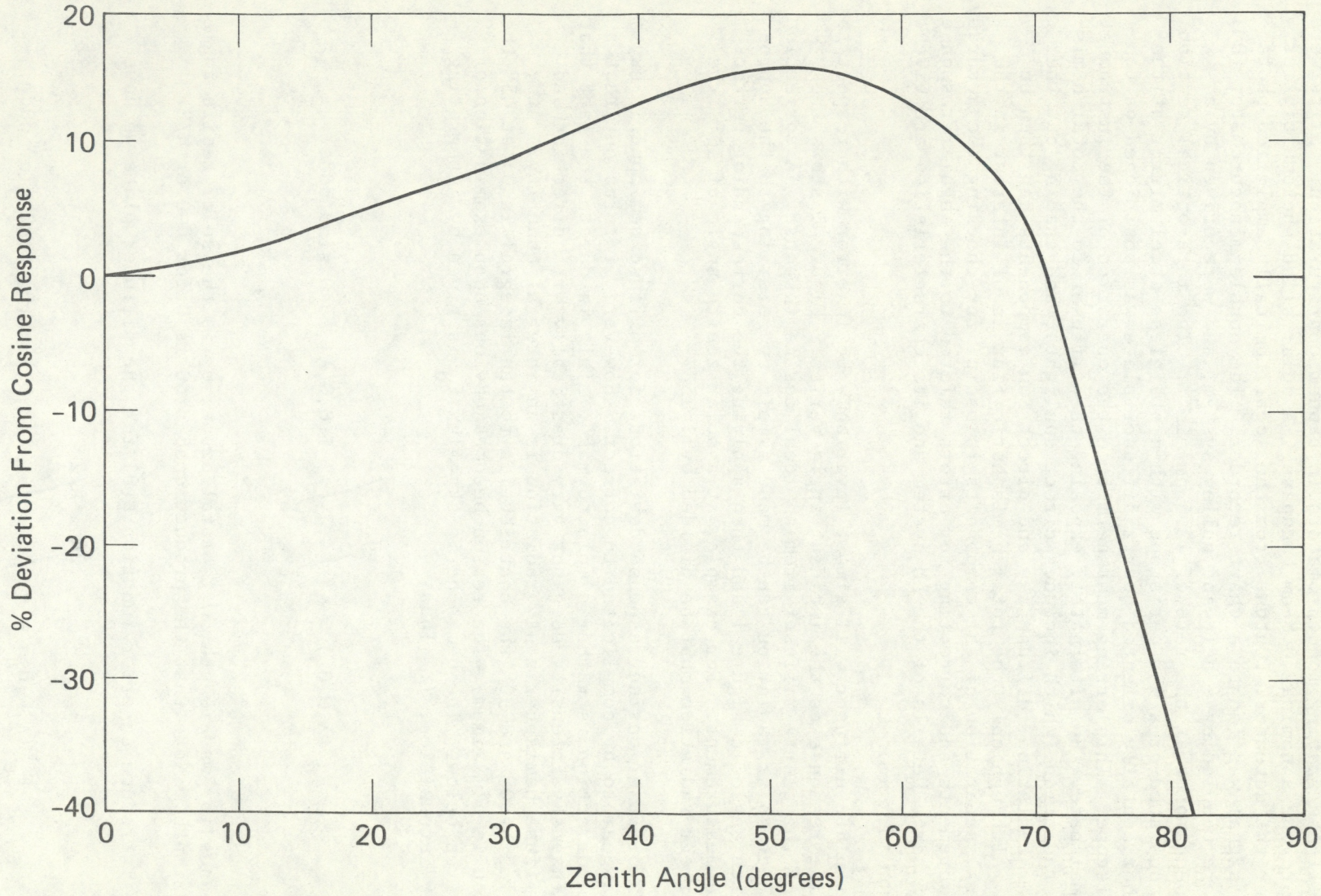

Figure 1.--Plot showing the percent deviation of the DM quartz diffuser plate from a pure cosine response. The response of the diffuser plate is normalized to a value of 1 at cos θ = 1, or when radiation is incident in a zenith angle direction normal to the plate.

We can define a correction factor by

$$K(\lambda,\Omega,\theta_o) = F_d(\lambda,\Omega,\theta_o) / F_\varepsilon(\lambda,\Omega,\theta_o).$$

To a first-order approximation we used for $I(\theta,\Omega,\lambda)$ Dave and Furukawa's (1966) tables for intensities as a function of zenith angle in the solar plane (azimuthal dependence is omitted). For λ = 307.5 nm, Ω = 0.340 cm, and θ_o = 60° a correction factor of 0.952. was derived. Now if we assume the sky intensities are isotropic (no dependence with direction) and perform the same integration, we arrive at a correction factor of 0.953 which amounts to a difference of 0.2%. This insignificant difference suggests that in the present work the correction for diffuse hemispheric flux need not be done with great care and that the assumption of isotropic sky intensities is sufficient for calculating correction factors for diffuse radiation. The solar aureole has not been included in the calculations because molecular scattering is so powerful in the uv that, under most circumstances, the aureole contribution is relatively small and can be neglected in the correction procedure. The procedure we use to correct for cosine response error no doubt is imperfect, and therefore a bias in our measurments may still exist between measurements made at different solar zenith angles.

In the UVB region the relative magnitudes of the diffuse and direct flux can change drastically with changes in solar zenith angle, wavelength, and total ozone. Table I illustrates this for varying solar zenith angle and wavelength. Note that between 30° and 60° solar zenith angle, a rapid change

Table I.--Values of direct and diffuse hemispheric flux for wavelengths 307.5 and 312.5 nm and solar zenith angles 0°, 30°, 60°, 75°, and 85°. All values are multiplied by π units of flux incident at the top of the atmosphere. Data are taken from Dave and Furukawa (1965). Subscript s stands for direct and d stands for diffuse.

θ_o \ λ	302.5		307.5		312.5	
	F_s	F_d	F_s	F_d	F_s	F_d
0°	1.034-1	7.832-2	3.308-1	2.510-1	6.428-1	4.755-1
30°	5.283-2	5.066-2	2.023-1	1.924-1	4.355-1	4.015-1
60°	1.703-3	5.628-3	1.742-2	5.010-2	6.577-2	1.706-1
75°	1.522-6	2.036-4	1.359-4	4.864-3	1.770-3	3.600-2
85°	2.681-18	7.088-5	1.666-12	5.037-4	3.400-9	2.485-3

Note: The numbers preceded by a minus sign are the powers of 10 that are used to scale their associated quantities; e.g., 1.522-6 = 1.522×10^{-6}

in the diffuse relative to the direct radiation is seen. This deviation will be seen in the response of a flux-measuring instrument if the diffuser departs from a cosine response. With this in mind, we have examined the error in the RB-meter using the published characteristics of its cosine response.

Figure 2 shows the deviation of the RB-meter's angular response from that of a cosine response, relative to the maximum at $\cos \theta_o = 1$, as obtained from Berger (1976). Corrections for the error for diffuse hemispheric flux were made for this cosine response in the same way as described for the DM. The diffuse flux response for the RB-meter was calculated to be 0.823 times the response of an ideal diffuser. Taking this into account, along with the characteristics of the direct and diffuse flux shown in Table I and the cosine response deviation of Figure 2, we calculated a net response at a wavelength of 312.5 nm. The results are shown in Figure 3 in which it is seen that the meter will read low under all circumstances. We see that the slope of the error curve is related to the relative contributions of the direct and diffuse flux. The direct flux plays a greater role at the smaller zenith angles, and the diffuse flux plays a greater role at the larger zenith angles. If the sky were completely overcast, the error would stay roughly constant at 0.823 at all solar zenith angles. The RB-meter cosine error was also calculated for $\lambda = 307.5$, which is close to peak erythema response. Little difference was seen when this error was compared with the diffuser error for $\lambda = 312.5$, which is close to a peak response of the RB-meter. An important point to note is that if the RB-meter is calibrated for high Sun conditions, this will change the relative magnitude of the cosine error curve so that it would probably be smaller than shown in Figure 2. The entire curve would be shifted closer to 1.0.

Even though there is a strong variation seen in the RB-meter cosine error in the range of $30° < \theta_o < 60°$, it is unlikely that it will be seen in the measurements. In this range of solar zenith angle, the uv flux falls off very rapidly as the angle increases; thus, a variation on the order of 10% will be obscured. It is demonstrated later in this report that for cloudless or nearly cloudless skies the RB-meter cosine error may be acting to improve the meter's ability to represent the true erythematogenic radiation because of the direction the error takes with increasing solar zenith angle.

To correct for the DM cosine response error, a procedure was used that gives ±10% accuracy. First, F_d is subtracted from F_t (the sum of direct and diffuse flux), yielding the direct component. Then, the direct component is corrected for the cosine error and added to the corrected diffuse component to produce a completely corrected, absolutely calibrated F_t value. Because the F_t and F_d measurements must be taken separately, a gap in time existed between the two measurements. Time coincidence is obtained by linearly interpolating numerical functions log F_t and log F_s vs. airmass, where F_s is the direct solar flux. Then, for any given airmass, F_t and F_s are defined for all wavelengths of interest. Some error noise on the order of ±10% in F_s may at times be introduced with this procedure.

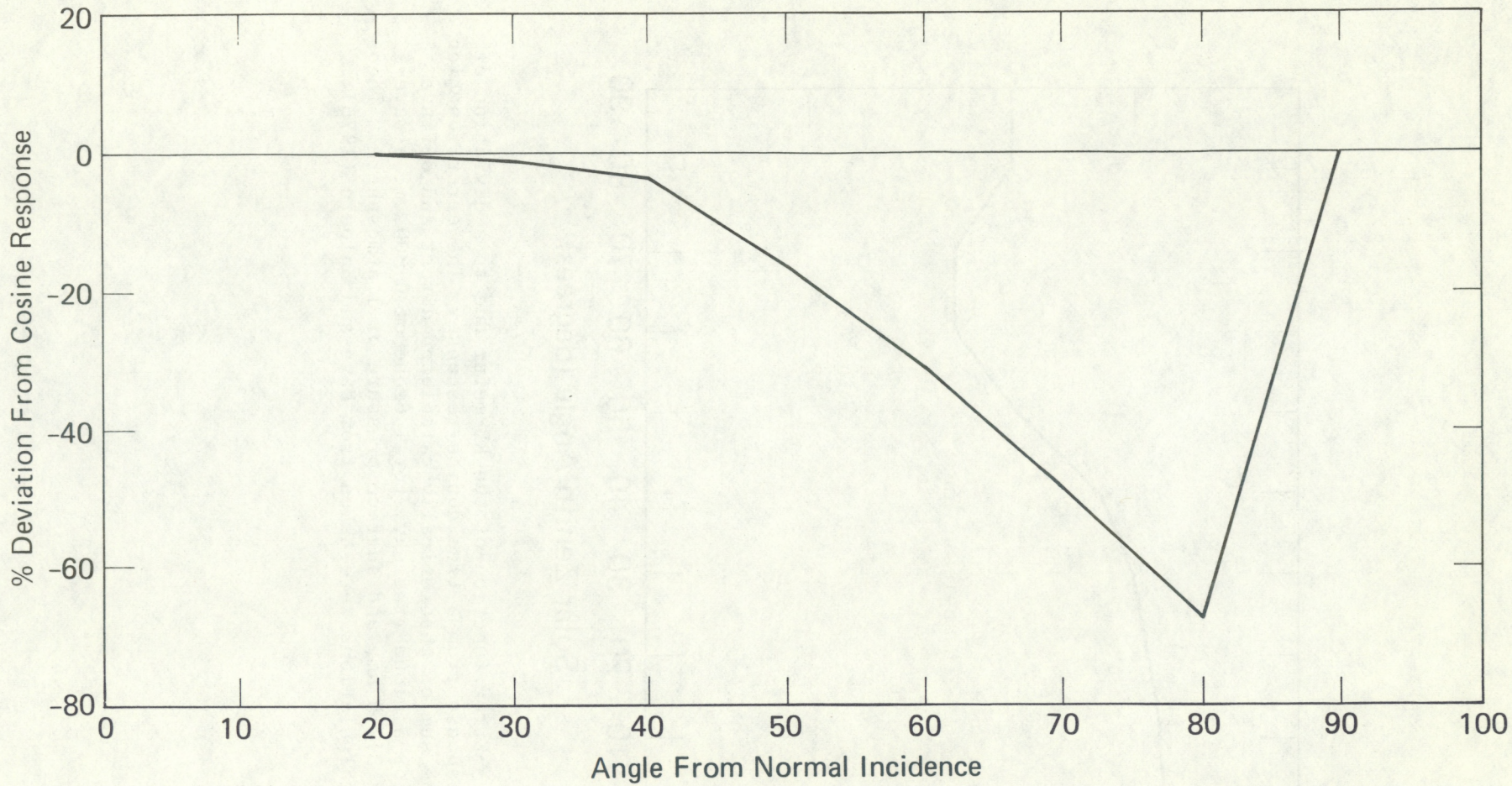

Figure 2.--Plot showing the percent deviation of the RB meter from a pure cosine response. The response has been normalized to a value of 1 at cos θ = 1, or when radiation is incident in a zenith angle direction normal to the sensing surface. Data taken from Berger (1976).

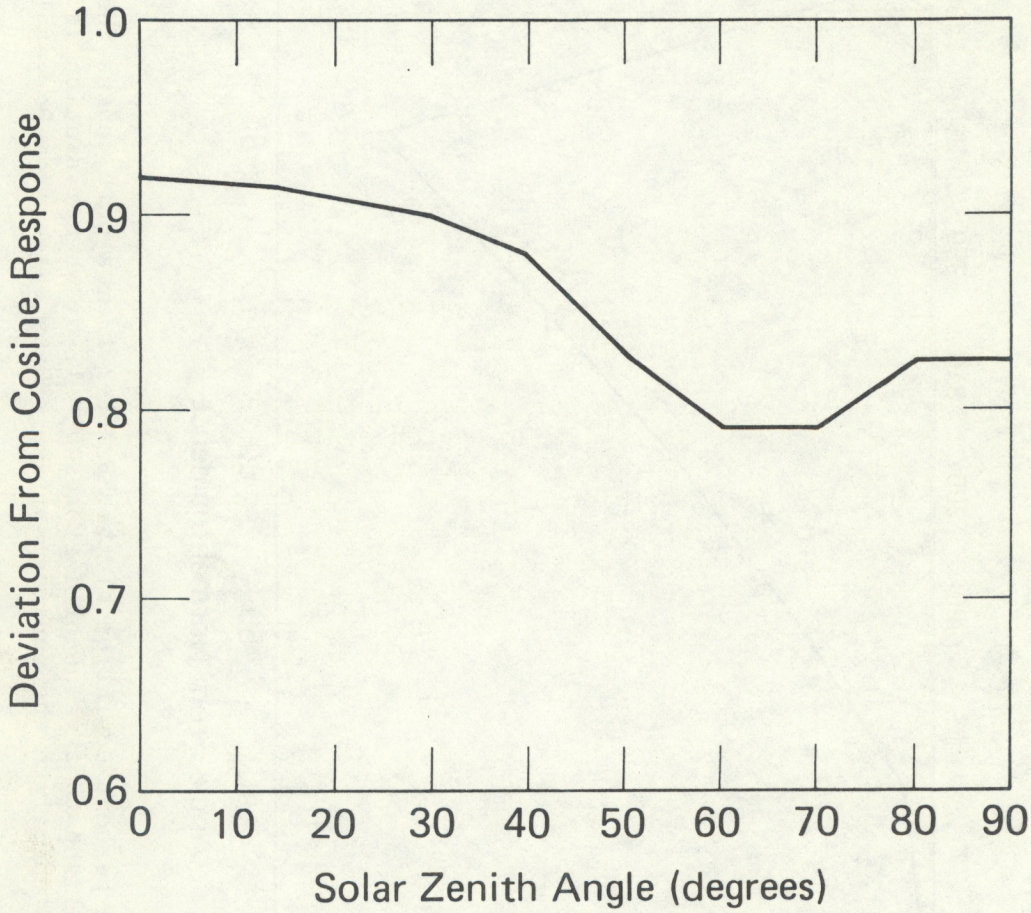

Figure 3.--Error function of the RB-meter due to a deviation of sensor response from a true cosine response. The error function is for the sum of theoretically calculated direct and diffuse fluxes, for a cloud-free sky, total ozone of 0.300 cm, a wavelength of 312.5 nm, and surface pressure of 1 atmosphere. Theoretical calculations were taken from Dave and Halpern (1976).

3. MEASUREMENT PROCEDURE

Measurements with the RB-meter and the DM were done concurrently when cloud-free sky conditions prevailed, although in some cases a few broken clouds were present, but these did not usually obscure the direct Sun. A few broken clouds are not likely to affect the diffuse sky radiation seriously in the uv because molecular scattering is so strongly involved.

The instrumentation was located on the highest roof of the ERL Laboratory in Boulder. Even at this location a few objects (mainly the air conditioner) were within the 2π field of view of the diffuser plate. Mountains to the west were also in view, the highest elevation being about 7° from the horizontal. This amounts to a solid angle obstruction of, at most, a few percent for a horizontal diffuser viewing a 2π hemisphere. The error due to the distant mountains is further diminished because multiply-scattered uv radiation originates in a narrow cone about the zenith direction above the point of measurement at surface (Sekara and Dave, 1961).

A good deal of practice and experimentation in the laboratory and on the roof was done before it was determined that the DM system was reasonably reliable. Five good sets (five episodes) of simultaneous RB-meter and DM measurements were obtained for evaluation purposes. DM data on strip charts were digitized for log-signal voltage vs. time. Signal voltage was converted into absolute units using the standard lamp calibration curves obtained in the laboratory. Chart time was converted into wavelength by determining the wavelength positions of several Fraunhofer lines and then calibrating the recorded travel rate for wavelength position with respect to time. To eliminate slack problems in the grating drive system the DM was always made to scan wavelength starting from the longest wavelength. Also, it was easier to define an approximate wavelength starting position at the longer wavelength since the signal was stronger. The DM was started near 400.0 nm, and the wavelength calibration starting position was visually set at 396.8 nm, which is one of the prominent Ca II lines in the Fraunhofer spectrum.

An uncertainty of about ±0.5 nm in wavelength position was encountered with the present DM system. An uncertainty of this magnitude will not normally present a serious problem with the end result, because the erythema bandpass is on the order of 6-12 nm, although some of the measurement noise undoubtedly will be due to the wavelength uncertainty. Details on calibration procedures are given in Appendix A.

Figure 4 shows a typical observation of the total flux (F_t) vs. wavelength for a solar zenith angle of 55° taken on the 13th of August. Figure 5 is a plot of the diffuse flux measured near the same time. The ordinates are in terms of the common logarithm of F, and the abscissas are wavelength in nanometers. We have estimated the uncertainty of the measured flux to be on the order of ±10% absolute, where perhaps this might occasionally be exceeded in the erythematogenic region of the uv spectrum. A number of factors contribute to the uncertainty; among these are sensitivity fluctuations within the instrumentation system, wavelength errors, changing atmospheric conditions such as ozone, turbidity and spotty cloudiness, observer errors (such as time), and data reduction procedures such as digitization of the chart record. Typically, a spectrum such as the one shown in Figure 5 is convoluted with both the erythema action spectrum published by Coblentz and

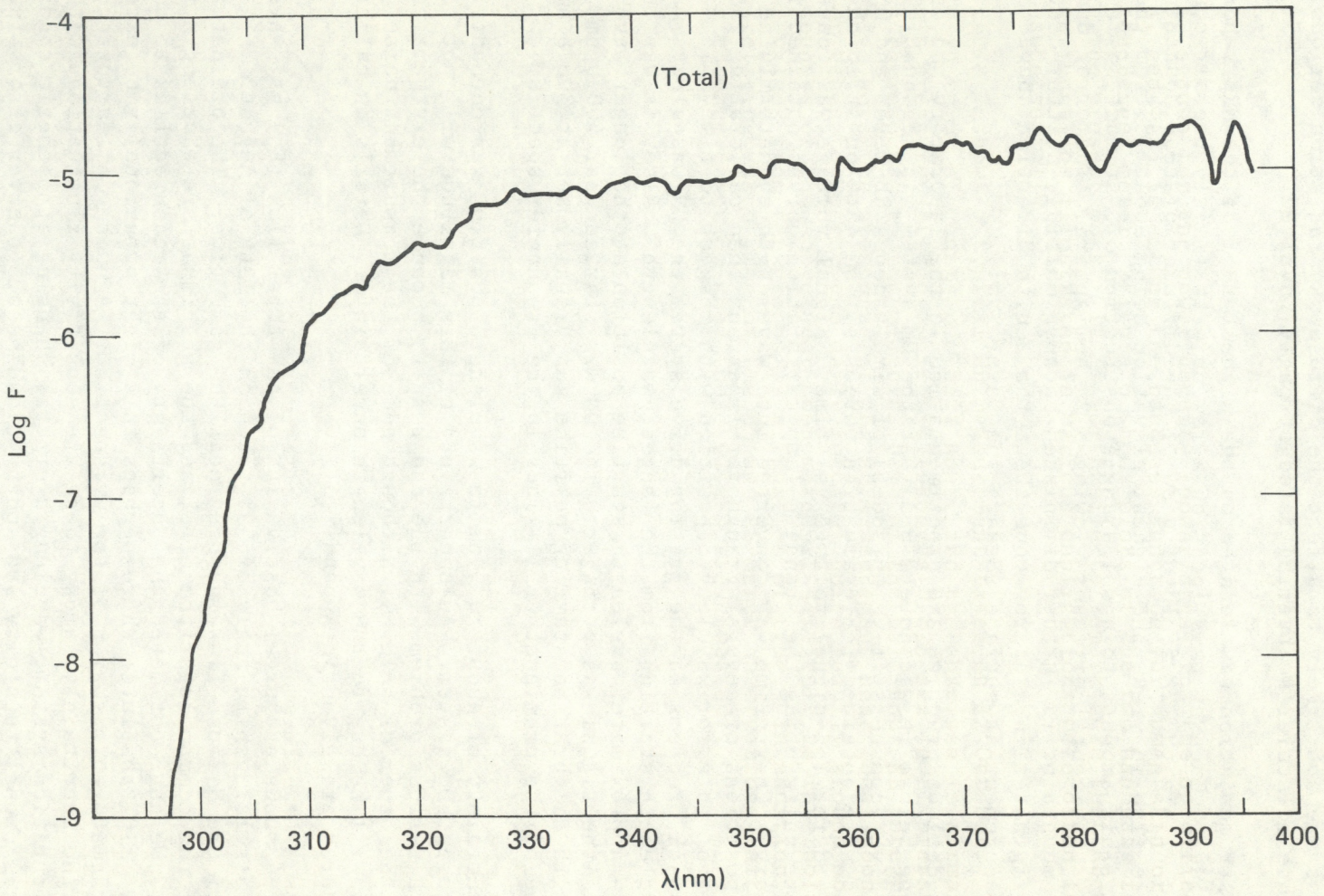

Figure 4.--Plot of logarithm of total uv spectral flux (F_t) vs. wavelength. Solar angle was 55°. The measurement was taken on October 13, 1978, at Boulder, Colo.

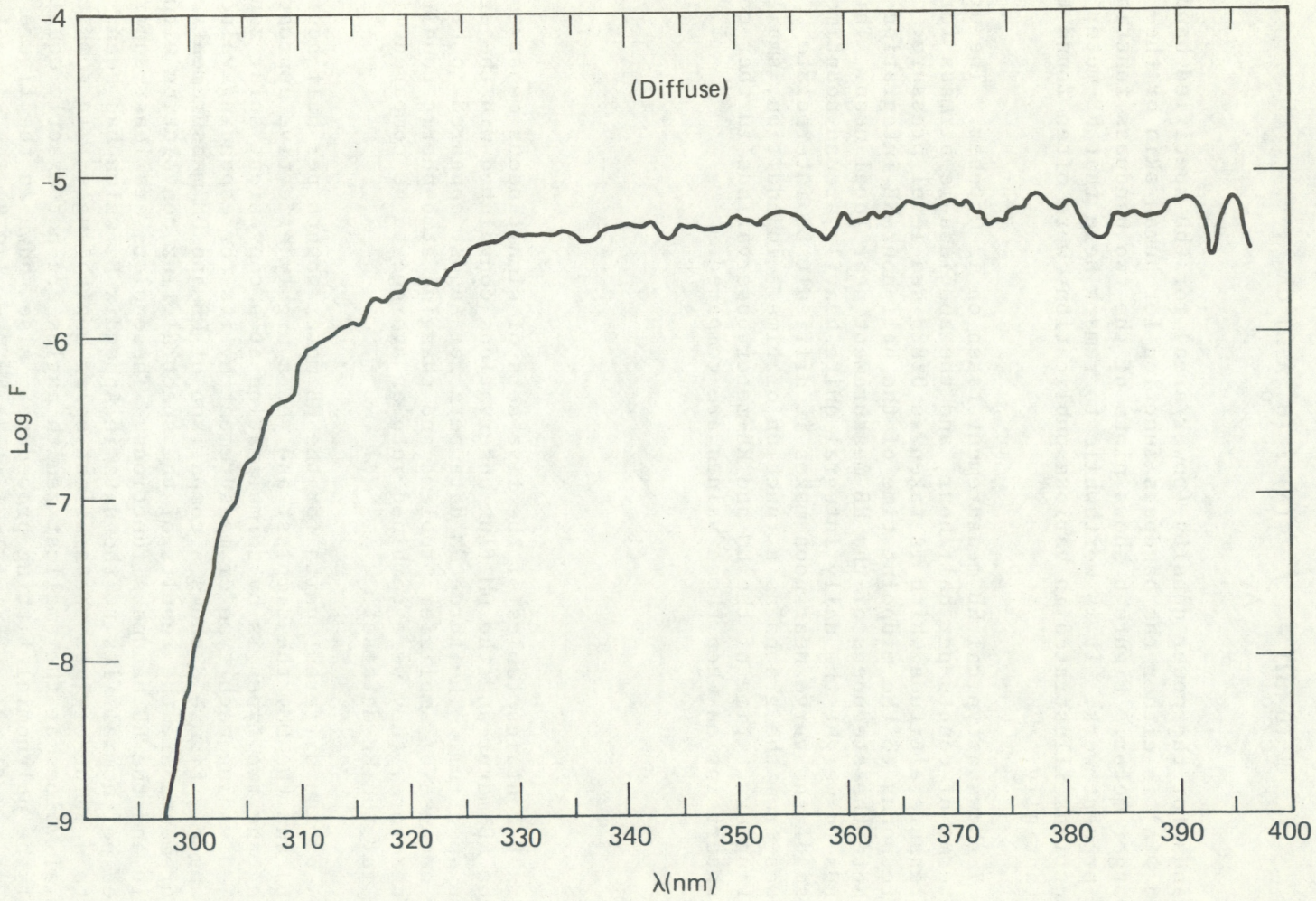

Figure 5.--Plot of logarithm of diffuse uv spectral flux (F_d) vs. wavelength. Solar zenith angle was 55°. The measurement was taken on October 13, 1978, at Boulder, Colo.

Stair (1934) and the bandpass curve of the Robertson-Berger meter (Green, 1975) to obtain estimates of absolute flux in the bandpass region. The convolution takes the mathematical form

$$E_c(\theta_o,\Omega) = \int_{\lambda_1}^{\lambda_2} \Phi(\lambda)\, F_t(\theta_o,\lambda,\Omega)\, d\lambda \quad ,$$

where E_c stands for the power density (power/area) for the specified band $(\lambda_2-\lambda_1)$, and $\Phi(\lambda)$ is either the bandpass function for human skin or the Roberston-Berger meter. Figure 6 shows plots of the two bandpass functions used in the present work. It is worthwhile to remark here that RB-meter bandpass functions illustrated in various publications were often found to differ substantially.

Figure 7 shows a typical RB measurement taken on 12 October. The ordinate is in terms of counts per half hour, and the abscissa is airmass for Boulder's pressure altitude which is taken as 0.825 sea level pressure. The airmass corresponds to the midpoint time of the half-hour RB integration interval. Note the steepness of the RB measurement near local noon. This behavior tends to weight the daily integral quite heavily around noontime. The steepness of the curve near noon makes it difficult to interpolate precise values from the graphs as a function of time. In addition, small errors relating exact time of the DM and RB-meter observations further contribute to uncertainties when these values are compared.

4. ANALYSES

Appendix B contains tables of the five sets of simultaneous measurements made with the RB-meter and the DM flux observations convoluted wih the erythema action spectrum. The three DM data sets for August appeared to be quite noisy because of amplifier problems and changing atmospheric conditions as well. Therefore, they were combined into an average to be compared with the average for the RB data set.

In view of the different units for the RB meter counts per half hour (Berger 1976) and the DM, the simplest and yet a highly effective approach for comparing the two types is by normalization at a convenient solar zenith angle, i.e., dividing each type of measurement by its corresponding value at the chosen angle. Figure 8 shows a comparison of RB and DM measurements. The DM measurements are the results of the spectral flux convolution with the erythemagenic and the RB bandpass functions. These plots are least-square second-degree polynomial fits to the data in Appendix B, which had been normalized to a value of 1 at the smallest solar zenith angle. In some cases the polynomial values at the smallest zenith angles are not exactly equal to 1 because of the polynomial fitting procedure. Also shown in the figure is a plot of results of theoretical calculations by Dave (1978) for a wavelength of 307.5 nm and a total ozone of 0.268 atm-cm. Because Dave's data were not for the same total ozone used here and the wavelengths differed somewhat, it was necessary to resort to interpolation (log interpolation with λ and linear

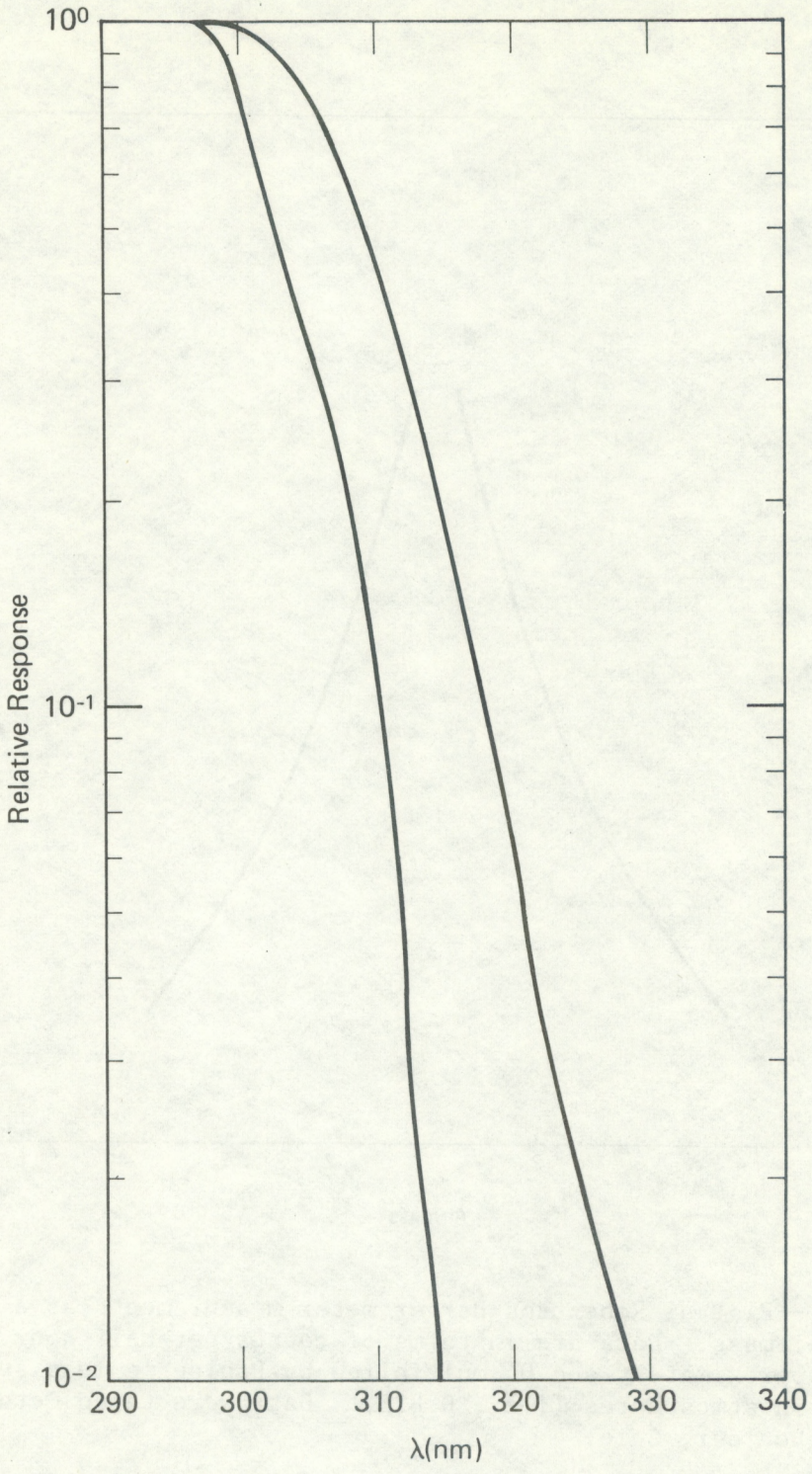

Figure 6.--Plots of human erythema action spectrum (left plot) and spectral response of the Robertson-Berger meter (right plot). Data for erythema action spectrum were obtained from Coblentz and Stair (1934). Data for the RB spectral response were obtained from Green (1974).

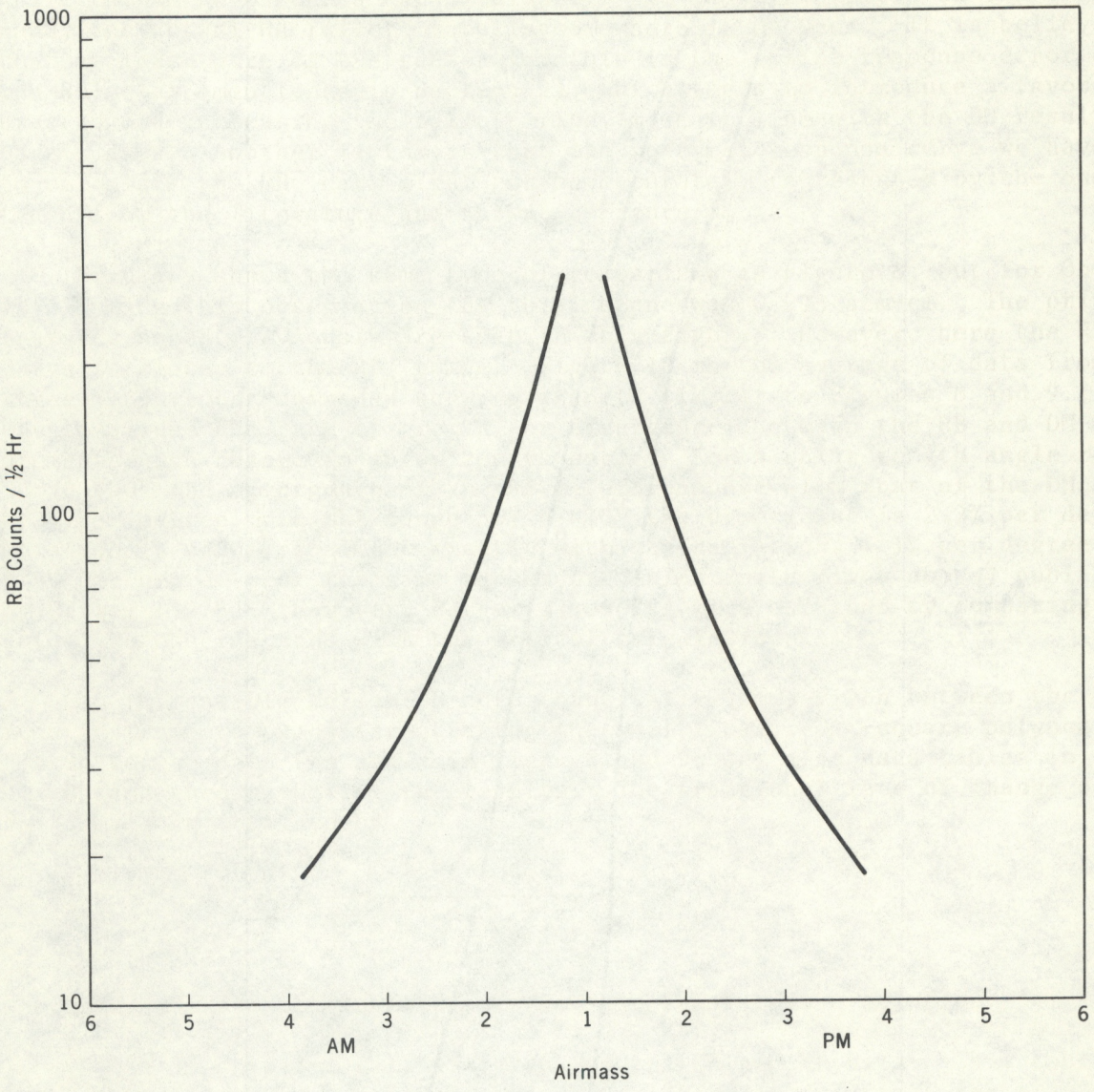

Figure 7.--Plot of Robertson-Berger meter measurements as a function of airmass. Data are in terms of counts per half hour. Airmass is approximately sec θ_o multiplied by Boulder's mean surface pressure in atmospheres (i.e., 0.825). Data were taken October 12, 1978, at Boulder, Colo.

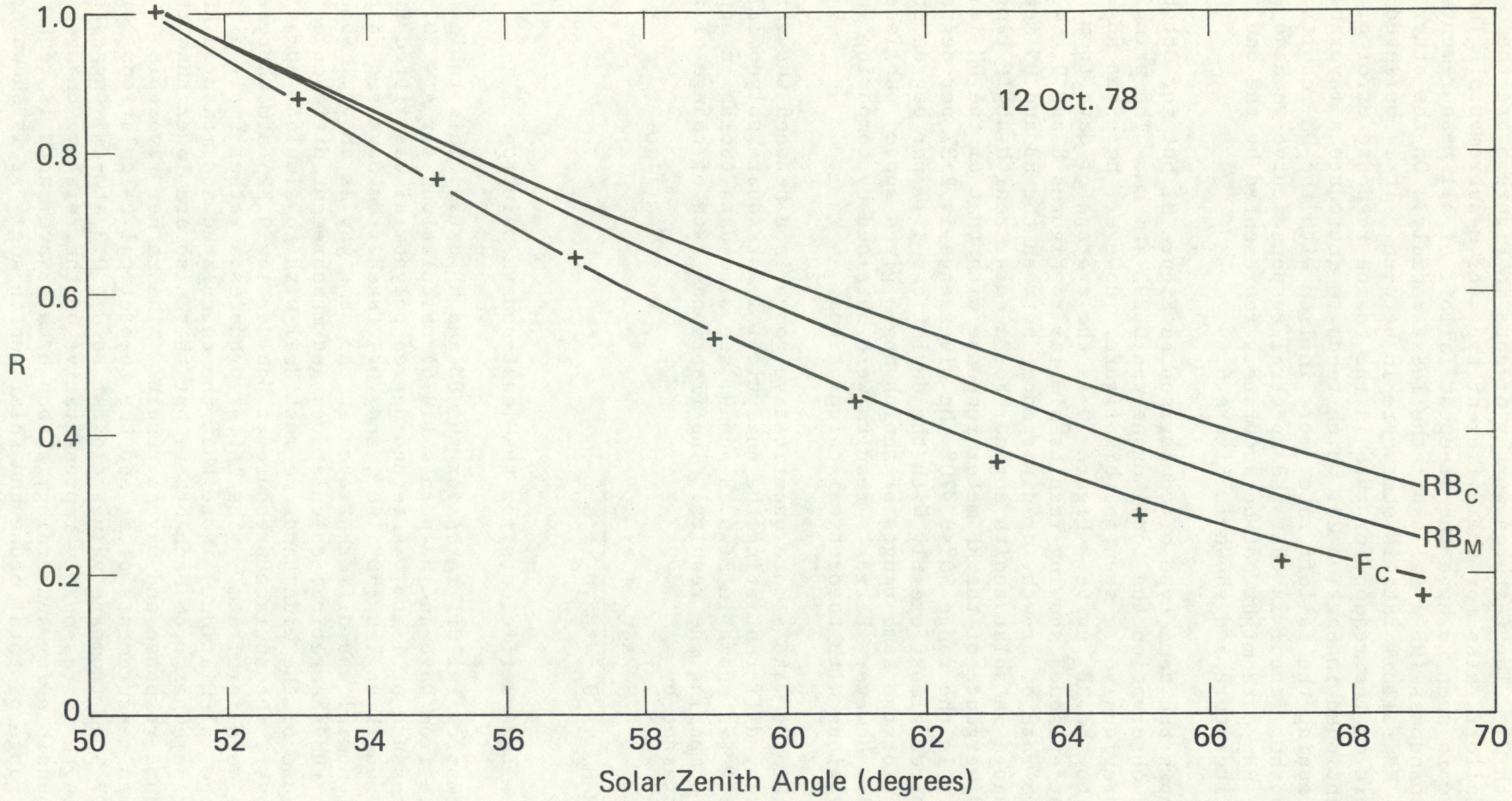

Figure 8.--Plots of uv data from various sources. E_c and RB_c were calculated from DM data, and RB_m is from data taken with the Robertson-Berger meter. The + marks are from calculations by Dave for Ω = 0.268 atm-cm and λ = 307.5 nm. All data were adjusted by a multiplier to give a value of 1 at the minimum solar zenith angle.

interpolation with Ω). The features worthy of note in Figure 8 are the differences in falloff rates for the different types of measurements. The DM erythema curve is seen to have the steepest falloff of all measurements while the DM-RB bandpass (RB_c) falls off the least rapidly. On the other hand, the actual RB falloff rate is somewhere in between. It is believed that at least part of the reason for this is the cosine response error of the RB-meter (mentioned in Section 2), which tends to introduce a favorable bias toward increasing the falloff rate, more in line with the DM results and Dave's data. Another factor is that the spectral response curve we have used to calculate the RB_c data might not be accurately represented by the one taken from the literature and shown in Figure 6.

Figure 9 shows the same type of comparison as Figure 8, but for October 13. During this observation the total ozone was 0.293 atm-cm. The principal features noted previously are seen in this figure. However, here the RB_c curve is closer to the RB_m curve. Figure 10 is the average of data from three measurement episodes showing results similar to Figures 8 and 9. We have examined the rate of growth, or divergence, between the RB and DM measurements with change in solar zenith angle. For a solar zenith angle range $30°<\theta_o<50°$ the divergence of the RB meter response with that of the DM is 1.2% per degree. In the range $50°<\theta_o<70°$ the divergence is 2.3% per degree. This result compares almost exactly with the deviations 1.1% per degree and 2.3% per degree (for the same ranges of zenith angle given above) published by Berger (1976). However, Berger's results were obtained by comparing actual RB observations with theoretical calculations.

It is possible to make a more quantitative comparison between the various instruments by differentiating the analytical least-square polynomial fitted to the data (as shown in Figs. 8 and 9; see also data tables in Appendix B) and then comparing the results. The fractional rate of change of flux per degree is obtained by

$$\frac{dR}{Rd\theta} = \frac{2a_2\theta_o + a_1}{a_2\theta_o^2 + a_1\theta_o + a_o} \quad ,$$

where the a's are the coefficients for the least-square solution.

Table II compares falloff rates for the DM and RB data. This table also shows an estimate from Dave and Halpern's (1976) calculations for λ = 307.5 nm and a surface pressure of 1 atm. A second-degree polynomial was fitted to flux values at three zenith angles (50°, 60°, and 70°) taken from Dave and Halpern's tables. The polynomial was differentiated in the same way as above. Some differences between the theoretical calculations and measurement differences can be expected because of the wide bands we must deal with to simulate human skin response. Moreover, the surface pressure at Boulder is ~0.825 atm whereas the calculations were for 1 atm. (The latter produces a rather small bias in the rate-of-change calculation.) Note that the calculated and measured RB responses differ somewhat from each other, but they also are lower than the calculated erythema response and Dave's results. The rather favorable comparison between measurements of E_c and the theoretical calculations for a wavelength of 307.5 nm (compare values closest to Ω = 0.3 atm-cm) suggests that this wavelength is reasonably representative of the relative changes in the uv flux responsible for sunburning, although this wavelength is restricted to a limited range of total ozone and solar zenith angle as is shown next.

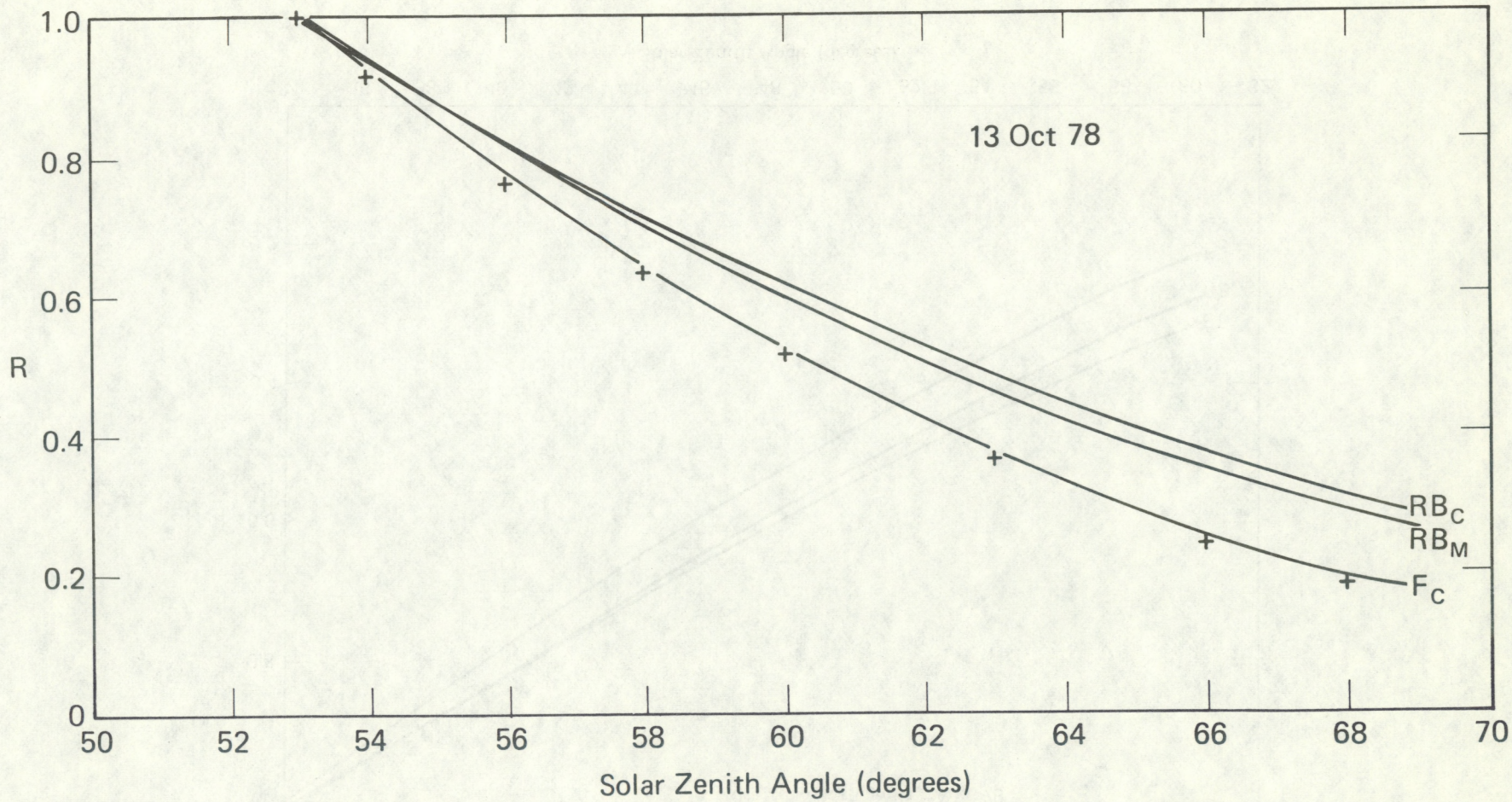

Figure 9.--Plots of uv data (as in Figure 8) for October 13.

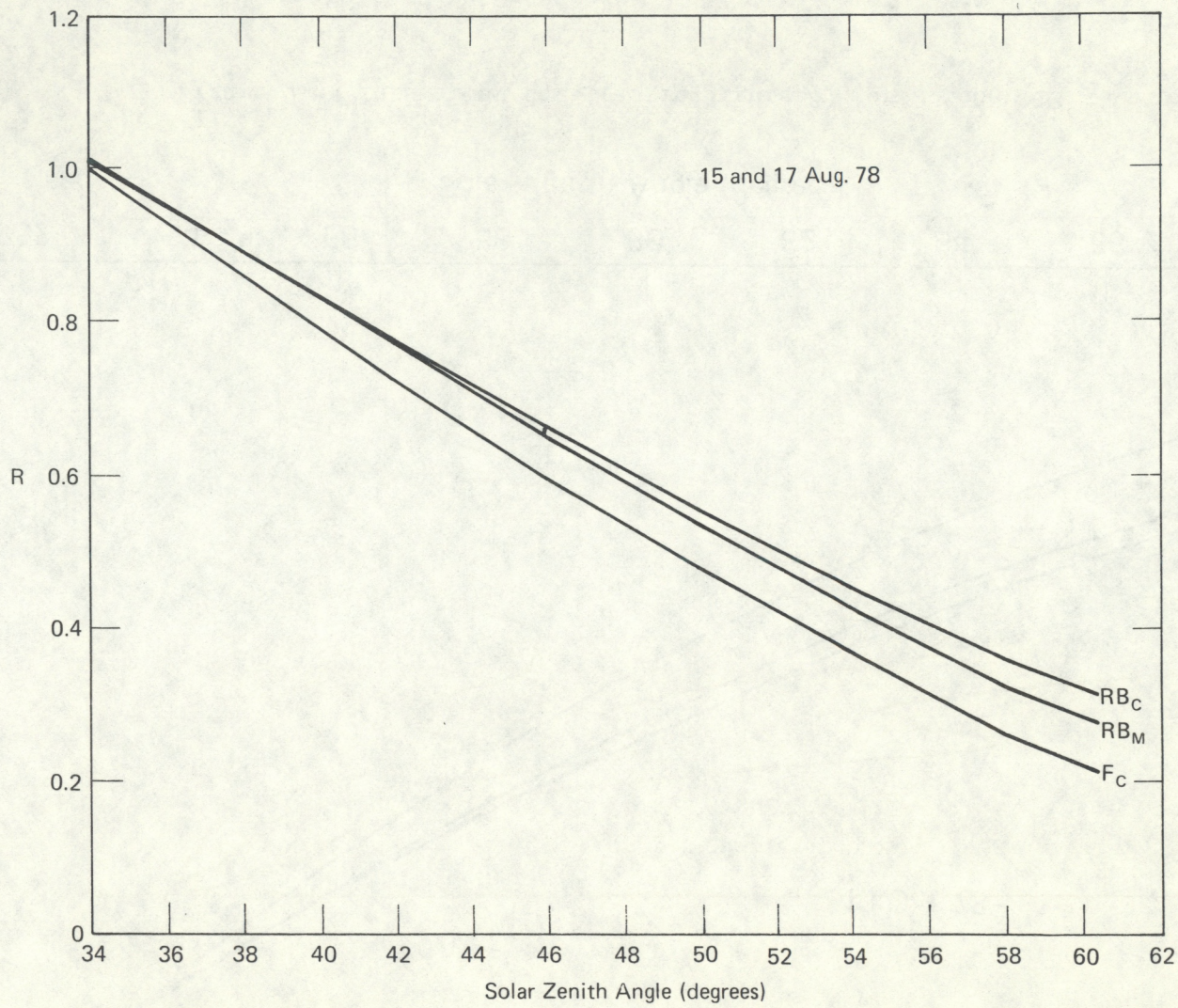

Figure 10.--Plots of uv data (as in Figure 8) for an average of three observational episodes: 1 on August 15, and 2 on August 17.

Table IIa.--Comparison of fractional rate of flux decrease with solar zenith angle for measurements at $\theta_o = 60°$. Units are in terms of fractional change per degree change in solar zenith angle. Dave's calculations are for total ozone of 0.3 cm, Rayleigh optical depth of 1.043, and aerosol optical depth of 0.09.

Date	Double Monochromator		RB-Meter	Total Ozone	Dave (Ω= 0.3)
	DM (deg^{-1})	RB_c (deg^{-1})	RB_m (deg^{-1})	Ω (atm-cm)	F' (deg^{-1})
15 Aug.(p.m.) 17 Aug.(a.m.) 17 Aug.(p.m.)	-0.116	-0.075	-0.091	0.314	-0.102
12 Oct.(p.m.)	-0.090	-0.062	-0.075	0.268	-0.102
13 Oct.(p.m.)	-0.108	-0.073	-0.084	0.293	-0.102

Table IIb.--Average magnification factors (% change in flux / % change in ozone) calculated from all data in Table IIa. The uncertainty in these is considered to be large.

	DM	RB_c	RB_m
Magnification	1.70	1.26	1.24

We have examined the integrand of the convoluted integrals to determine the wavelength at which the integrand is a maximum. Figures 11 and 12 illustrate the shape of the integrand functions for human skin and the RB-meter response. Note some interesting Fraunhofer structure in these functions. In an attempt to quantify certain characteristics of the integrand functions, wavelengths of peak power for the erythema and RB response functions and wavelengths for their half-power points were selected as criteria for comparing characteristics of the two types of instruments. Table III summarizes these wavelengths for solar zenith angles of 30°, 50°, and 70°. The data in this table illustrate the distortion of the spectral distribution of uv radiation incident on the skin as solar zenith angle changes. There is likewise a similar distortion that takes place when total ozone changes; however, this aspect was not examined since the Fraunhofer structure, in combination with measurement noise, is difficult to deal with because of the limited sample size and the rather small changes in ozone associated with the present set of measurements. The data in Table III indicate that the half-power bandpass of the RB meter is approximately 4.1-5.2 nm wider than the

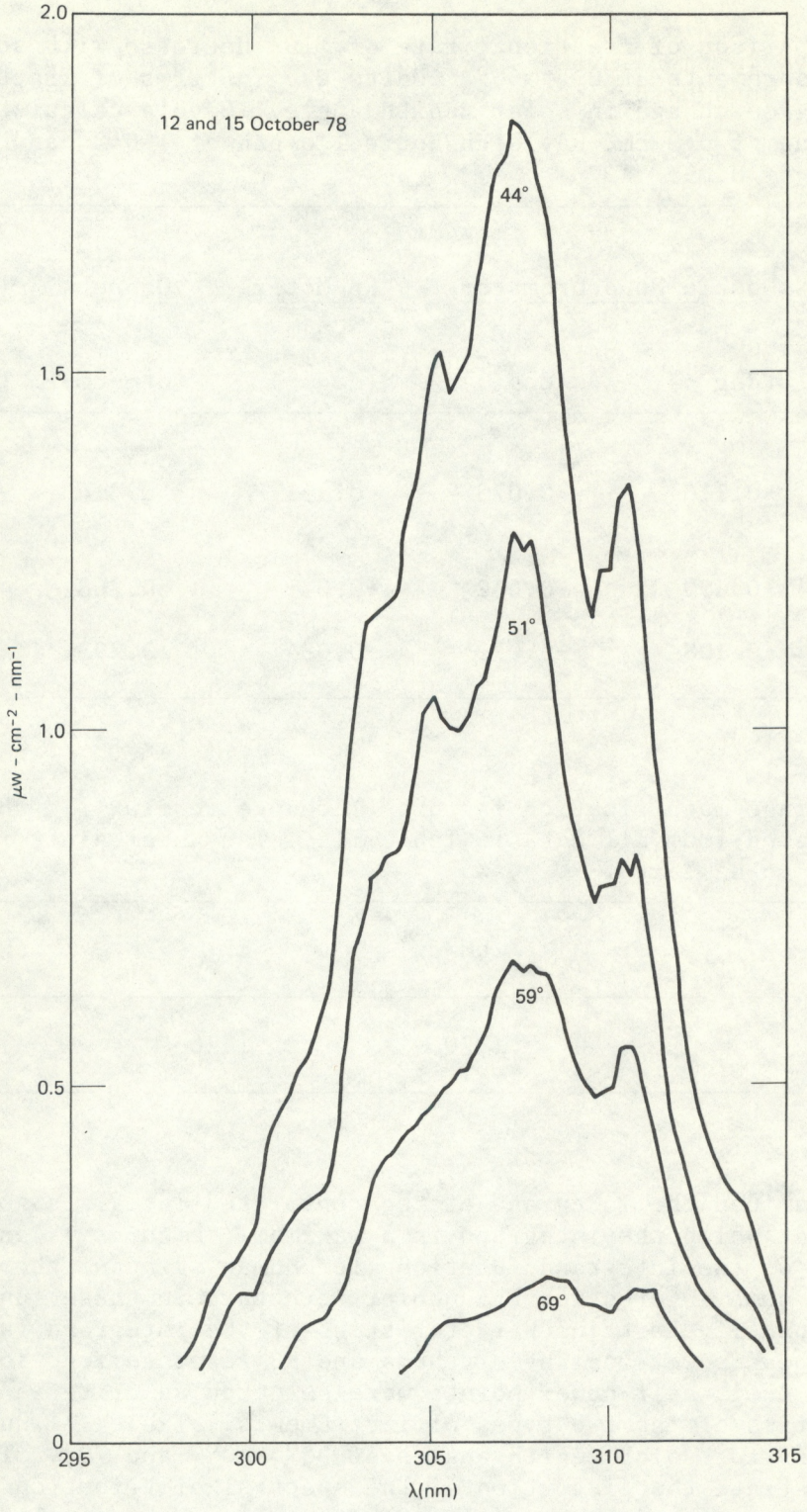

Figure 11.--Function of spectral flux irradiating human skin. Estimated from DM measurements convoluted with the human action spectrum relative to unity response at 297.0 nm (Coblentz and Stair, 1934).

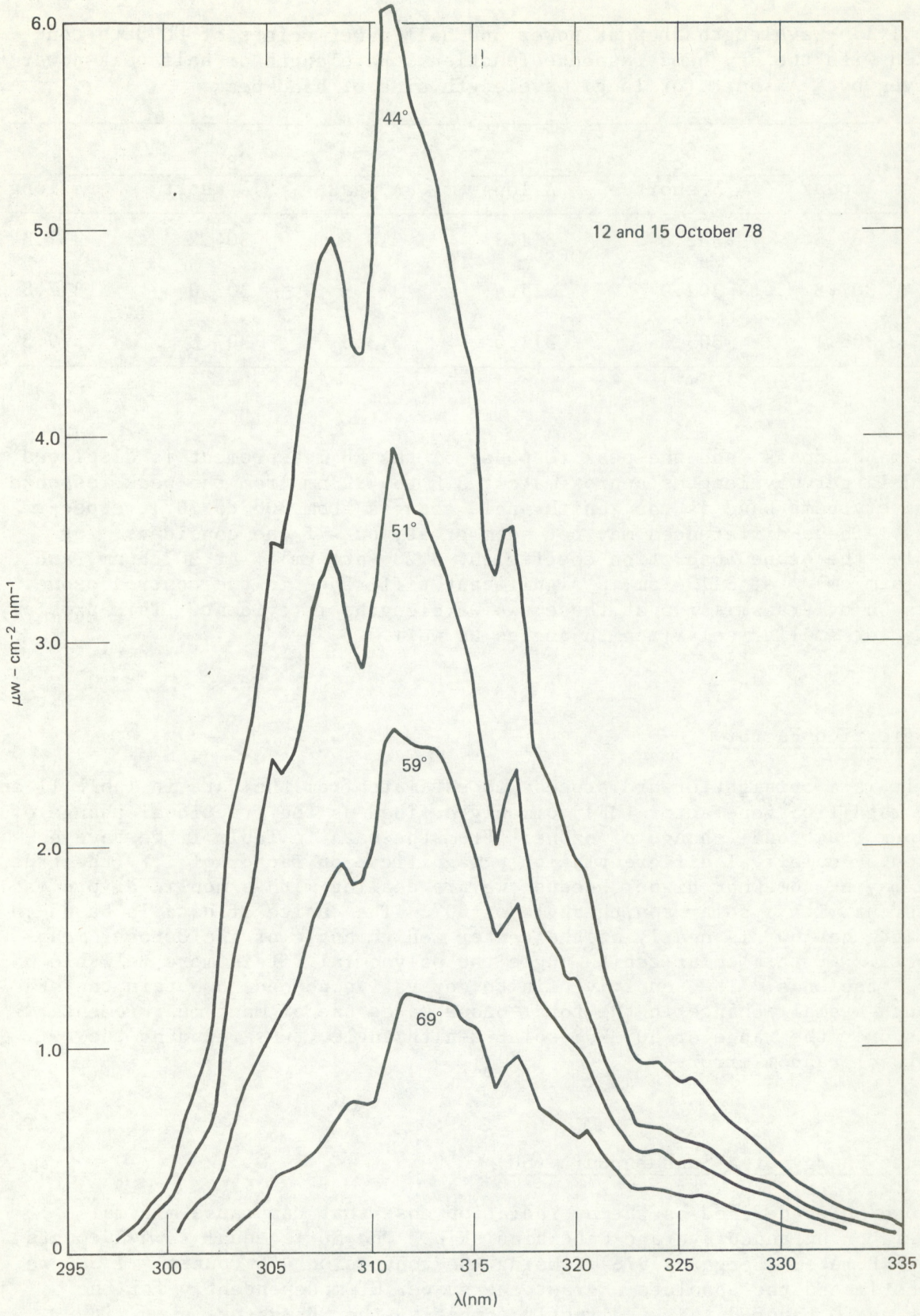

Figure 12.--Function of spectral flux detected by the Robertson-Berger meter. Estimated from DM measurements convoluted with the published response curve for the RB-meter.

Table III.--Wavelength at peak power and half-power points of DM data convoluted with the erythema response function. Wavelength of half peak power is given by ½ λ short (or long) wavelength side of band peak

	E_c			R_{Bc}		
	λ peak	½ λ short	½ λ long	λ peak	½ λ short	½ λ long
30°	307.3	302.3	311.3	310.8	304.2	317.3
50°	307.8	302.9	311.4	311.3	305.0	317.8
70°	308.1	305.3	311.6	313.0	307.8	319.3

erythema bandpass, and the peak response of the RB measurement is displaced toward larger wavelengths approximately 3.5 to 4.9 nm from the peak response of the erythema band as the zenith angle changes from 30° to 70°, respectively. These differences may not seem great, but if one considers, for example, the ozone absorption coefficient 3.28 $(atm\text{-}cm)^{-1}$ at 307.8 nm, and 2.07 $(atm\text{-}cm)^{-1}$ at 311.4 nm, a significant difference in the control ozone exerts on uv transmission at these two wavelengths is evident. This problem exists for smaller solar zenith angles as well.

Magnification Factor

It is a straightforward process to estimate from the data in Table II an ozone magnification factor (MF) commonly defined as the fractional change of flux per fractional change of ozone. From the data in Table II we have estimated by numerical differentiation a magnification factor of 1.7 (the true value may be somewhat higher because we are dealing with a nonlinear process) consistent with a solar zenith angle of 60°. The choice of data is based on the fact that 60° is nearly at the center zenith angle of the October measurements. At this solar zenith angle the polynomial fit is more reliable than at the ends. The sensitive finite derivative needed to obtain the MF for such a small change in the total ozone makes use of many measurement points over the range of 50°-70° solar zenith angle, thus reducing the effects of random error.

Absolute Energy of a Sunburn Unit (SU)

One SU is defined as the uv radiation dose that can cause minimal erythema on untanned average Caucasian skin. One SU is equal to 440 counts on the RB-meter (Berger, 1976). Using the conversion 440 counts = 1 SU, we have estimated the absolute radiant energy per SU independently for the August and October data, by directly comparing the RB measurements with estimates of E_c. The two sets were then matched at $\theta_o = 50°$ (because a difference between the two existed, presumably because of differences in

Table IV.--Absolute energy per sunburn units (SU) relative to 297 nm from various sources.

Value	Comments	Source
$15\pm(1\text{-}2)$mJ cm^{-2} SU^{-1}**	Estimated from daily integrals*	Machta et al. (1975)
(18-24)mJ cm^{-2} SU^{-1}**		Berger (1979) private communication
24 mJ cm^{-2} SU^{-1}		Luckiesh (1946)
33 mJ cm^{-2} SU^{-1}	Theoretical value	Paltridge and Barton (1978)
40 mJ cm^{-2} SU^{-1}	$20° \lesssim \theta_o \lesssim 30°$	Caldwell (1975)
$(35\pm4 \rightarrow 20\pm2)$mJ cm^{-2} SU^{-1}**	$\theta_o = 30° \rightarrow 69°$	Present study

*Spread roughly estimated from the spread seen in a plot of RB vs. erythemal data

**Referenced to the response of an RB-meter

total ozone), after which a second-degree polynomial was fit to the composite set. Because the RB and DM measurements show a strong deviation with increasing solar zenith angle, we plotted uv energy per SU as a function of solar zenith angle. Figure 13 shows this plot. It is obvious that there is a considerable deviation between the RB and DM data as the solar zenith angle changes. Moreover, the characteristics of this curve are likely to change when the total ozone is substantially different. For these reasons, care should be exercised when comparing RB measurements made at different latitudes and seasons if the purpose is for human erythema studies. The polynomial function for the plot in Figure 13 is given by

$$\chi(\theta_o) = -0.00528\theta_o^2 + 0.144\theta_o + 35.5 \quad .$$

Data from various sources on the absolute uv energy for one SU are summarized in Table IV. The quantities identified by an asterisk were determined with respect to the response of an RB-meter. All other quantities were determined with respect to degree of reddening of untanned human skin. The rate of reddening vs. uv exposure can vary considerably. Berger (private communication) commented that the variability seen in sunburning of human skin has been observed to range from as low as 10 mJ cm^{-2} SU^{-1} to 24 mJ cm^{-2} SU^{-1} on various subjects. However, the commonly observed range is 18-24 mJ cm^{-2} SU^{-1}. He also noted that the peak response of the skin to uv radiation may vary from 294 to 298 nm.

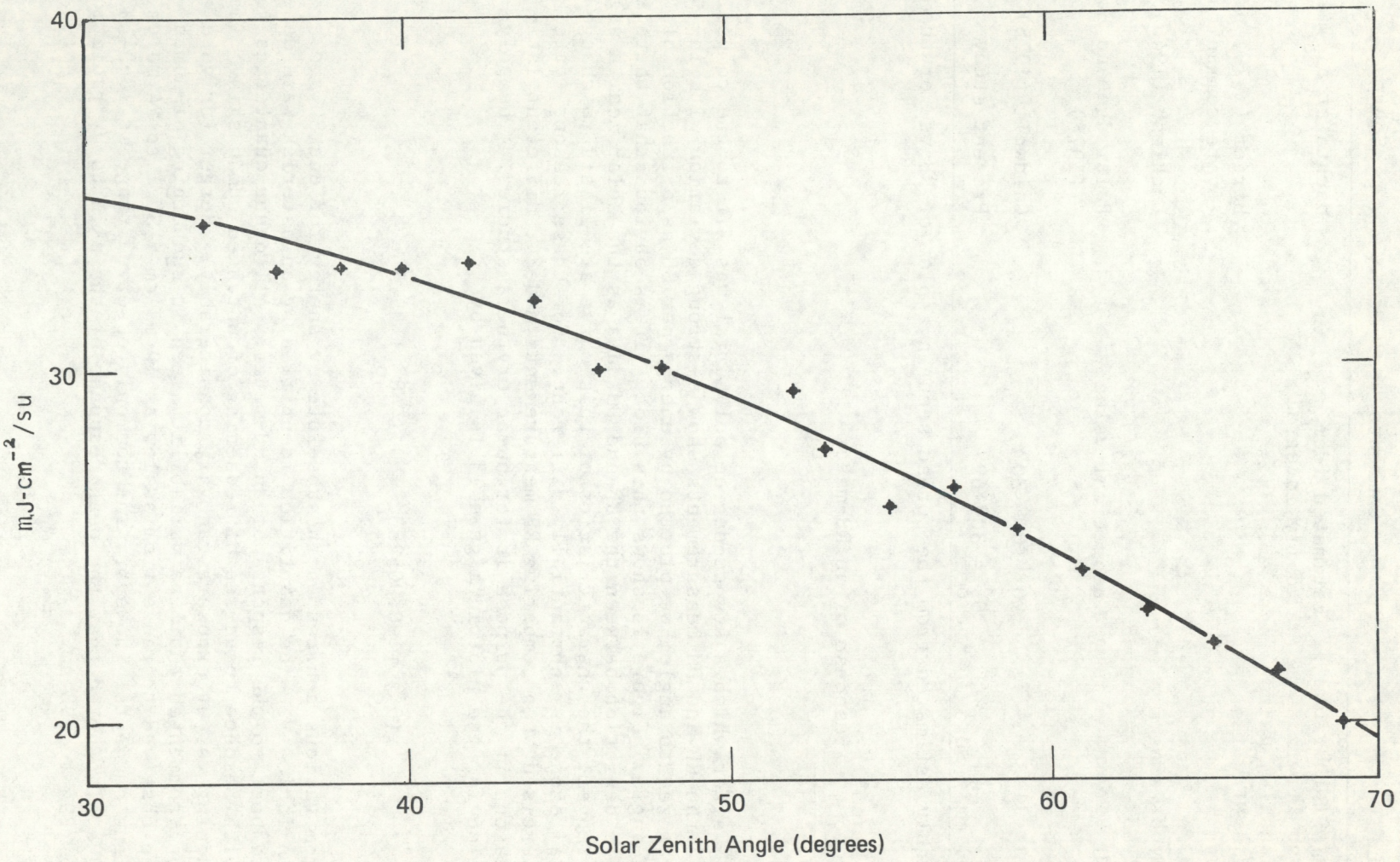

Figure 13.--Plot showing the absolute energy per sunburn unit (SU) vs. solar zenith angle θ_o. Standard deviation of the fitted points is 0.6 of an ordinate value. Uncertainty of the plot is ~ ±10%.

A few further comments are in order to qualify the values given in Table IV. Since the deviation of the RB-meter measurement from a true erythematogenic radiation will increase with increasing solar zenith angle, then a comparison of daily totals of each (as done for example by Machta et al., 1975) will result in the RB-meter measurements being too high (thus giving lower absolute flux values in the erythema band). Another consideration is that some of the values in Table IV were derived from laboratory experimentation, i.e., directly irradiating human skin and observing changes in redness, whereas other values were derived from direct comparison with the RB-meter. It is obvious that the calibration of a meter for average human skin is complex. The estimate of uncertainty in the DM results (i.e., ±10%) is made on the basis of error analyses on the DM observations. This uncertainty estimate does not reflect any uncertainty connected with the RB-meter observations which, from our limited experience, appear to correlate unsatisfactorily with the total ozone on a day-to-day basis; however, the sample size was small and reading errors might have introduced errors large enough to obscure the relationship.

5. CONCLUSION

The present study has two valuable aspects. The first is the development of a straightforward procedure for evaluating the performance of a Robertson-Berger (RB-meter) ultraviolet photometer. Similar instruments could be evaluated in the same way. The procedure was used in the present investigation to gather only preliminary information on the performance of the RB-meter, viz., for the case of cloud-free skies and fairly low total-ozone conditions, and for solar zenith angles between 30° and 70°. The second is the quantification of the response of the Robertson-Berger in terms of absolute energy units. It was found that at a solar zenith angle of 30°, 1 SU is equivalent to 35 ±4 mJ cm^{-2} and decreases nonlinearly with increasing solar zenith angle so that at 69°, 1 SU is equivalent to 20 ±2 mJ cm^{-2}, all values being relative to the action peak at a wavelength of 297 nm. The variation with solar zenith angle is caused by the RB-meter's imperfect simulation of the erythematous response of human skin. The deviation of the RB-meter response with change in solar zenith angle is consistent with the RB-meter characteristics reported by Berger (1976).

When interpreting the response of the RB-meter in terms of human erythematogenic radiation, certain biases must be accounted for. For example, Bismarck, N.D., is at a latitude of 46.5°N and the latitude of Tallahassee, Fla., is 30.3°N. In midsummer (at maximum solar declination) the noontime solar zenith angles at these locations are 23.1° and 6.9°, respectively. The bias in RB-meter measurements between these two stations is about 6.2% (Tallahassee relatively lower), for hypothetically identical atmospheric conditions at each station. On the other hand, in midwinter at minimum solar declination, the noontime solar zenith angles are 69.9° and 53.3° for Bismarck and Tallahassee, respectively. The RB data bias between these stations for this time of the year is 48%, because the error difference is increasingly greater for increasing solar zenith angle. Again the comparison is for hypothetically identical atmospheric conditions. In addition to the deviation for identical atmospheric conditions, the bias is likely to be larger in actuality because

total ozone, being higher at Bismarck, will introduce a larger bias yet, compared with Tallahassee. All of these estimated biases are based upon RB-meter characteristics published by Berger (1976).

The summer vs. winter observations compared at individual stations will also suffer biases. At Bismarck the winter solstice data will be approximately 116% higher, relative to the summer solstice data, and at Tallahassee this difference will be approximately 54%, again for hypothetically identical atmospheric conditions at the respective stations and during summer and winter seasons. Since total ozone is higher in winter than summer, the deviation will probably be even larger. When considering the comments above, one must keep in mind that the sunburning rate is highly dependent on the Sun's zenith angle; i.e., most burning occurs during summer noontime.

A broader scope of performance evaluation of the RB-meter would entail studies of effects of clouds and changes in ground albedo, altitude, and total ozone. The same procedure used in the present investigation would apply to an extended evaluation; however, the accumulation of a necessarily much larger data set would require an automated uv instrument such as that used by Machta et al. (1975).

Because the RB-meter senses changes in uv radiation affected by ozone, aerosols, and clouds, this information within the data itself makes it likely that it can be used with appropriate transformations to estimate uv values for other kinds of action spectra. Evidence lending support to this is seen in the good correlations of uv radiation in specific wavelength bands located near the RB band with the RB radiation itself (Machta et al., 1975). Perhaps use could be made of ancillary data, such as total ozone observations, to improve the estimate. Any attempt to do this would require a sizable effort to collect sets of concurrently measured uv spectra and RB-meter data for a wide range of atmospheric conditions. To some extent this has been done by Machta et al. (1975).

If a need arose for high spatial resolution uv flux data say for a uv climatology of the globe, satellite systems such as the SBUV might be able to supply such data. However, a sizable research effort would be needed to develop the inversion algorithms for estimating flux at the bottom of the atmosphere, given satellite observations of total ozone, surface reflectivity, and cloudiness.

6. ACKNOWLEDGMENTS

A note of thanks is expressed to Richard Lehman for the loan of the double monochromator system, to Barry Bodhaine for constructing the logarithmic amplifier, and to Herb Kroehl for generously digitizing the chart recorder data. Thanks is also expressed to Dan Berger for his helpful conversations. We are indebted to Lester Machta for making this work possible.

7. REFERENCES

Berger, D. S., 1976. The sunburning ultraviolet meter: design and performance. Photochem. and Photobiol., 24, 587-593.

Caldwell, M., 1975: Sunburn units as measured by the Robertson sensor. CIAP Monograph No. 5, Appendix E, U.S. Dept. of Transportation.

Coblentz, W. W., and R. Stair, 1934. Data on the spectral erythemic reaction of the untanned human skin to ultraviolet radiation. Research Paper RP631, National Bureau of Standards Journal of Research, 12, January.

Dave, J. V., 1978. (Personal communication) The data used in Figures 8 and 9 were taken from a set of calculations done by Dave for a GMCC project dealing with aerosol errors to Umkehr measurements.

Dave, J. V. and P. Halpern, 1976. Effect of changes in ozone amount on the ultraviolet radiation received at sea level of a model atmosphere. Atmos. Environ., 10, 547-555.

Dave, J. V. and P. M. Furukawa, 1966: Scattered radiation in the ozone absorption bands at selected levels of a terrestrial, Rayleigh atmosphere. Meteorol. Monographs, 7, Amer. Meteorol. Soc., Boston, Mass., 353 pp.

Green, A. E. S. (Chairman), 1975: Expected changes in climatic variables and UV radiation. CIAP Monograph No. 5, Chapter 2, U.S. Dept. of Transportation.

Luckiesh, M., 1946. Applications of germicidal, erythemal and infrared energy. Van Nostrand, New York, 463 pp.

Machta, L., G. Cotton, W. Hass, and W. Komhyr, 1975. Erythemal ultraviolet solar radiation and environmental factors. Proceedings of the Fourth Conference on the CIAP, U.S. Dept. of Transportation, DOT-TSC-OCT-75-38, Cambridge, Mass.

Paltridge, G. W. and I. J. Barton, 1978. Erythemal ultraviolet radiation over Australia--the calculations, detailed results and input data. Div. Atmos. Phys. Tech Paper No. 33, CSIRO, Australia.

Sekara, Z. and J. V. Dave, 1961. Diffuse transmission of solar ultraviolet radiation in the presence of ozone. Astrophys. J., 133, 210-227.

APPENDIX A

CALIBRATION OF THE DM SPECTRAL RADIOMETER

Calibration of the absolute response of DM consists of three parts:

(1) Calibration of the wavelength position.
(2) Determination of the effective bandpass and its shape.
(3) Calibration for absolute flux response.

Calibration for wavelength position is easily done by exposing the instrument to a mercury lamp which emits strong line radiation at known wavelengths. Figure A1 is an example of a chart record made during a wavelength scan. The chart record is then referenced against the wavelengths of the known mercury emission lines. This serves to calibrate the instrument's wavelength meter.

The instrumental bandpass at the half-power points is found by measuring the wavelength width (at half power) of a well-defined feature in Figure A1. Note that the chart record is for a log scale. It is assumed that the mercury emission line is infinitely thin compared with the DM bandpass. Care was exercised to ensure that the features used to obtain the bandpass did not contain multiple mercury lines. The DM bandpass measured by this technique was consistently found to be 0.78 nm, which compares favorably with the manufacturer's specification of 0.8 nm for the set of slits that was used. It is acknowledged that other techniques may be used to measure the bandpass; however, the one now used is the simplest by far, since an alternate approach would require the use of a nearly pure monochromatic radiation source that can be varied over a spectral region that exceeds the bandpass of the DM. This would require the use of specialized instrumentation, unavailable at this laboratory.

Finally, the absolute flux calibration was accomplished with the use of a 1000-watt quartz-halogen, tungsten coiled-coil filament lamp (1000-W DXW), bearing the designation V-30 and supplied by the National Bureau of Standards.

A plot of the lamp's spectral irradiance at a distance of 50 cm is shown in Figure A2. Figure A3 shows a plot of the DM's response to the standard lamp.

Amplification of the photomultiplier output was accomplished with a logarithmic amplifier constructed by Barry Bodhaine of GMCC. The expressions used to convert chart readings of actual measurement episodes are as follows:

1. For direct radiation we have

$$F_s(\lambda) = K(\theta_o)C(\lambda)\, 10^{R_t(\lambda) - R_c(\lambda)} \{1-10^{R_d(\lambda) - R_t(\lambda)}\} ,$$

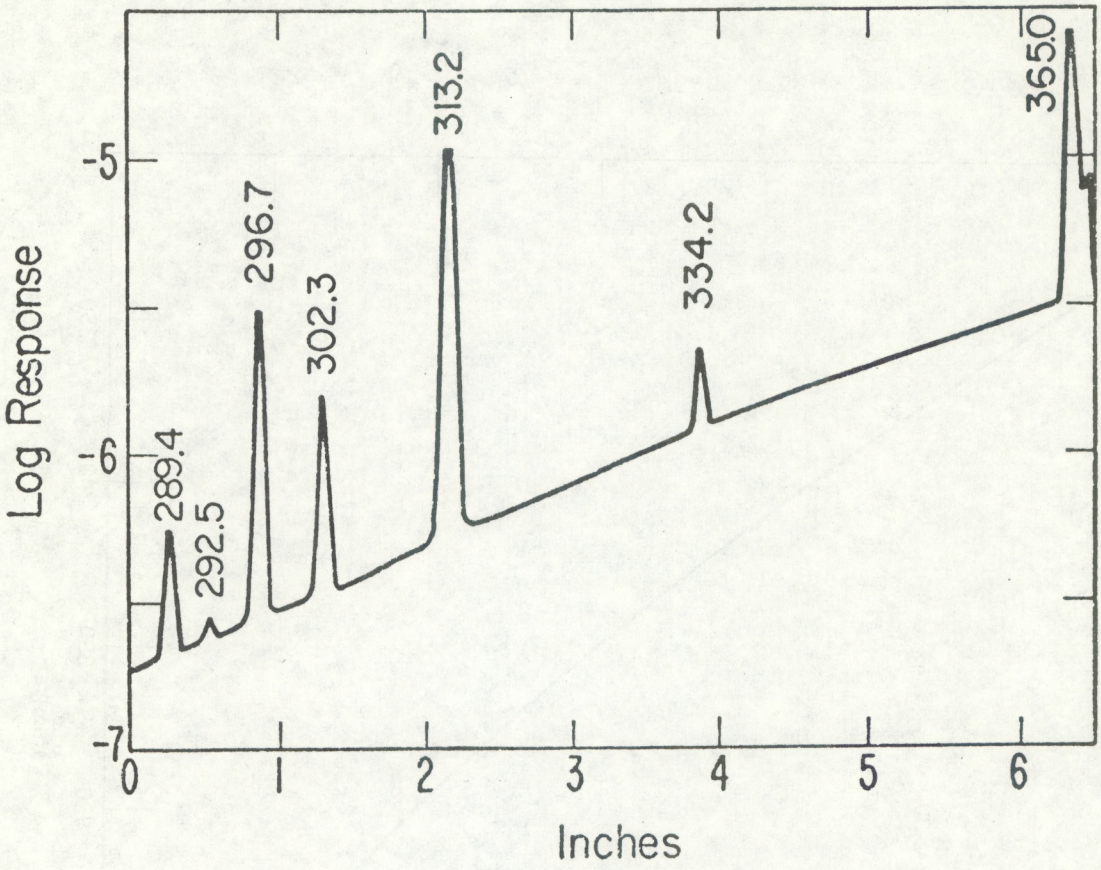

Figure A1.--Scan of a mercury source superimposed on the standard lamp source to calibrate the DM for wavelength vs. chart distance.

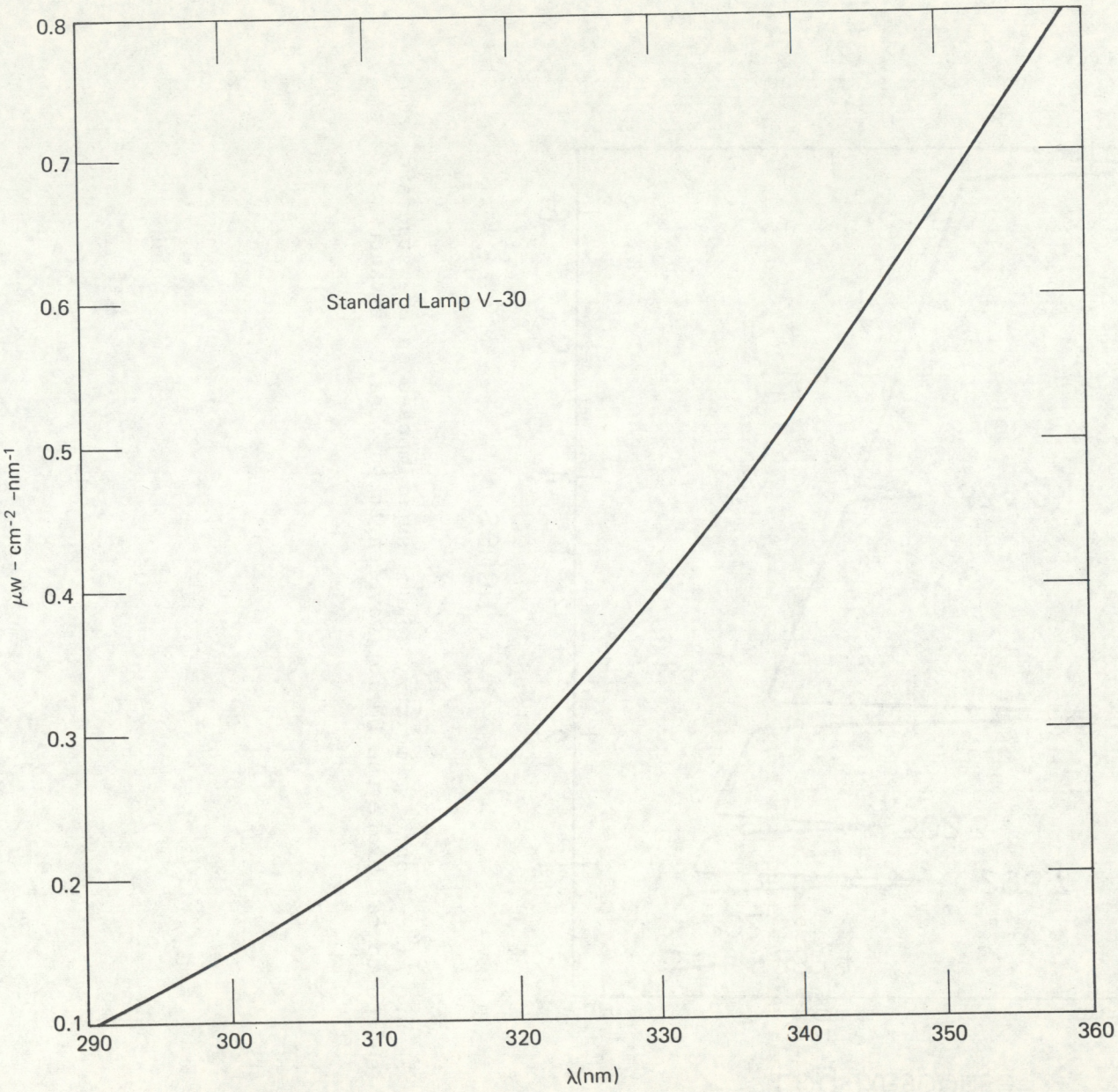

Figure A2.--Plot of standard lamp V-30 spectral irradiance.

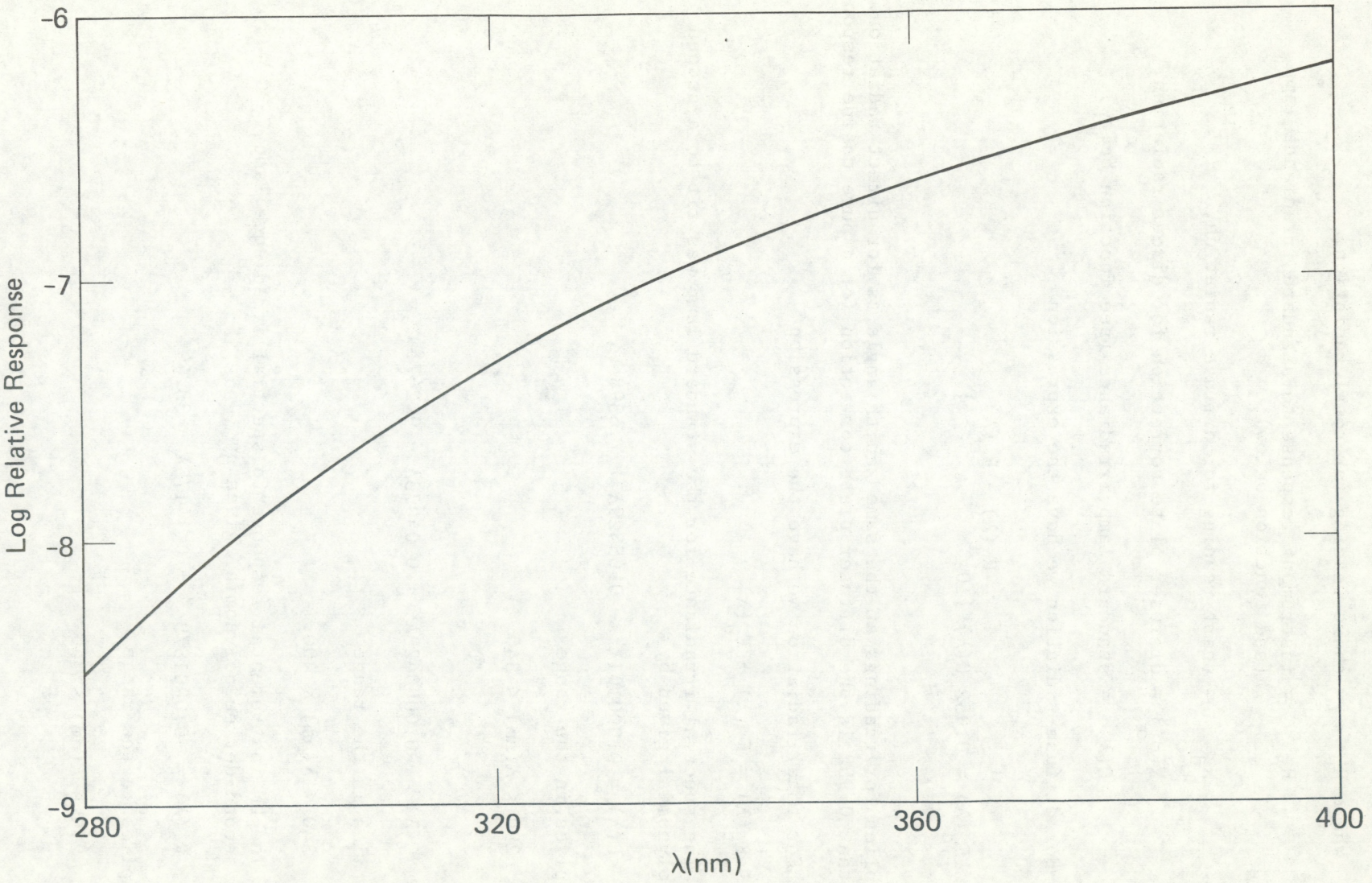

Figure A3.--DM response to spectral irradiance lamp.

where R_t = chart reading for total radiation,

R_c = instrument response to standard irradiance lamp (see function below),

R_d = chart reading for diffuse radiation,

$K(\theta_o)$ = diffuser plate correction for direct radiation,

$C(\lambda)$ = standard lamp irradiance (see function below).

2. For diffuse radiation we have the expression

$$F_d(\lambda) = 0.952\ C(\lambda)\ \{10^{R_d(\lambda) - R_c(\lambda)}\} \quad ,$$

which applies for readings at the same zenith angle as for direct radiation. The constant 0.952 is the diffuser plate correction for a pure cosine response.

3. For total radiation we have the expression

$$F_t(\lambda) = F_s(\lambda) + F_d(\lambda) \quad .$$

4. The spectral irradiance for the standard lamp was fit to a second degree polynomial given by

$$C(\lambda) = 0.000101\lambda^2 - 0.05529\lambda + 7.6398 \quad ,$$

which applies in the range

$$290 < \lambda(\text{nm}) < 340$$

and

$$C(\lambda) = -0.0000423\lambda^2 + 0.04073\lambda - 9.2471 \quad ,$$

which applies in the range

$$340 < \lambda(\text{nm}) < 400.$$

5. The DM instrumental response to spectral irradiance lamp V-30 was fit to a second-degree polynomial given by

$$R_c(\lambda) = -0.0001875\lambda^2 + 0.14175\lambda - 33.49 \quad ,$$

which applies in the range

$$290 < \lambda(\text{nm}) < 340$$

and

$$R_c(\lambda) = -0.0000823\lambda^2 + 0.07334\lambda - 22.391 \quad ,$$

which applies in the range

$$340 < \lambda(\text{nm}) < 400.$$

Figure A4 is a schematic diagram of the periscope and double monochromator arrangement. Because of light leaks in the DM's entrance assemblies, access ports, and wavelength meter ports, the entire system was wrapped in black cloth allowing only the periscope to be exposed to atmospheric uv radiation.

Verification of our measurements is difficult because we have not been able to make a side-by-side comparison with another instrument. However, we have attempted to check our measurements by making some comparisons of the DM measurements with theoretical calculations and experimental results. Figures A5 and A6 show two comparisons for wavelengths at 305.5 and 311.4, respectively. These theoretical calculations were done several years ago by DeLuisi at NCAR using the method of Dave and Furukawa (1966) for a molecular atmosphere without aerosols. In these comparisons the theoretical calculations turn out to be higher than the observed values. In view of the uncertainties such as aerosol effects, ozone absorption coefficients, extraterrestrial flux, and surface albedos, the agreement is reasonably good. Aerosols will probably reduce the downwelling flux by about 5%-10% at a solar zenith angle of 60%. (Recall the aerosol optical depth was 0.27 at λ = 380 nm on October 12.)

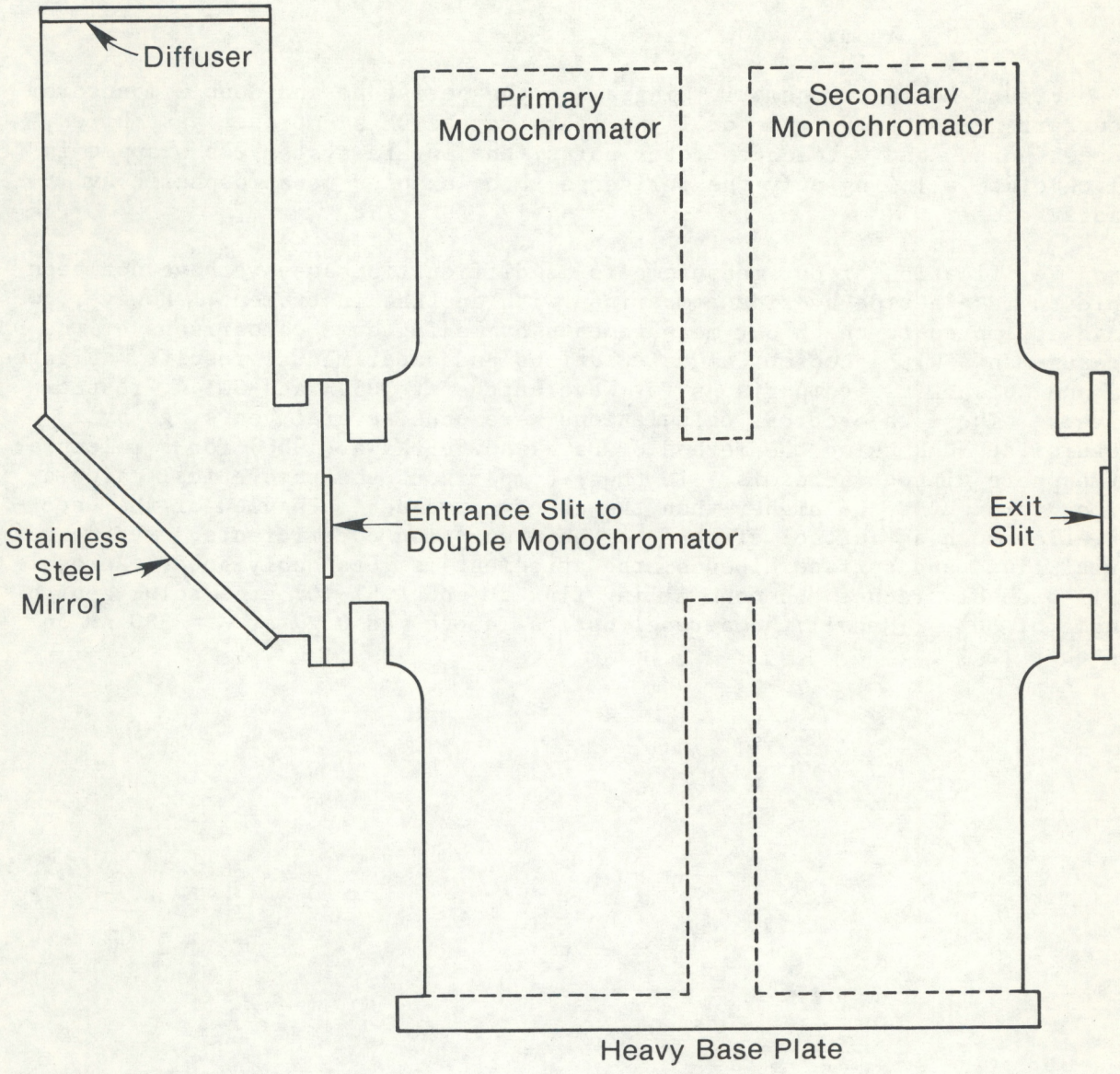

Figure A4.--Schematic of the periscope attached to the DM.

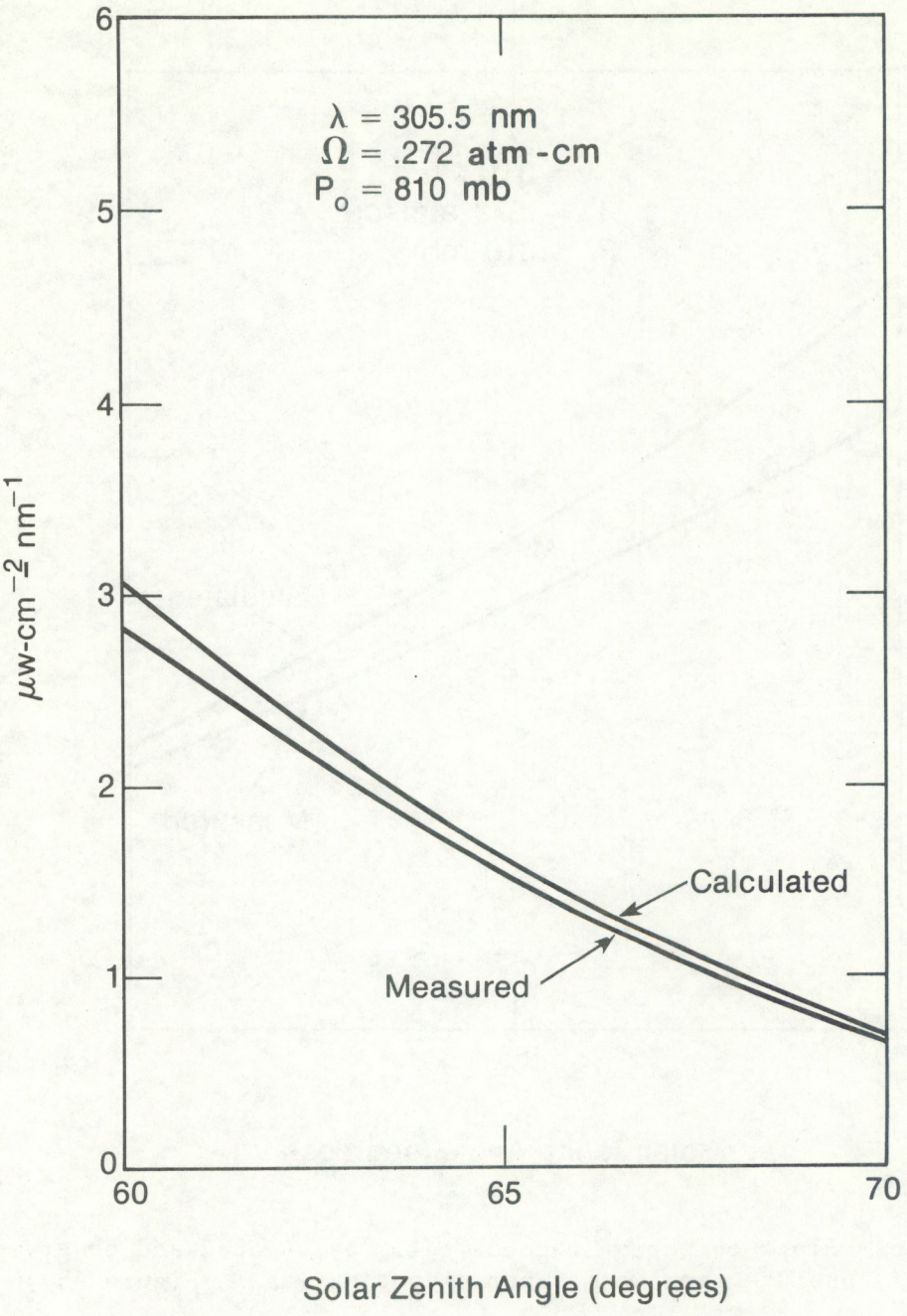

Figure A5.--Plots comparing theoretically calculated and observed values of absolute total hemispheric uv flux for similar atmospheric conditions.

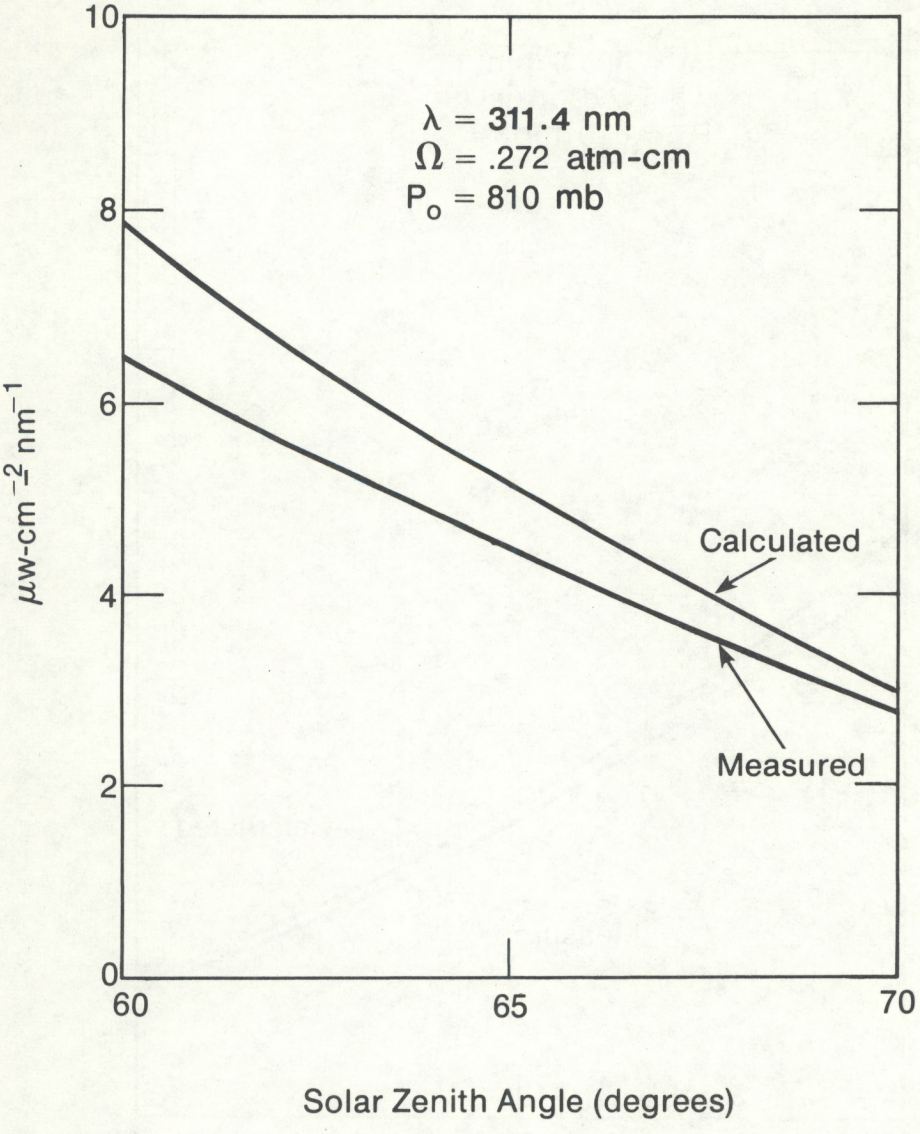

Figure A6.--Plots comparing theoretically calculated and observed values of absolute total hemispheric uv flux (as in Figure A5).

APPENDIX B

Tables of uv observations made concurrently with the RB and DM instruments. Data from these tables are used for the present research.

E_c = estimated absolute erythematogenic flux ($\mu W\ cm^{-2}$) using DM observations.

RB_c = estimated absolute flux ($\mu W\ cm^{-2}$) in the RB bandpass using DM observations.

RB_m = Robertson-Berger meter measurements (counts per half hour).

Ratios = ratio of the value at any solar zenith angle to the value at the smallest zenith angle.

Ω = total ozone

δ = aerosol optical depth.

August 15, 1978 (a.m.)

θ_o	E_c	RB_c	RB_m	Ratio E_c	Ratio RB_c	Ratio RB_m
34	23.97	115.0	475	1	1	1
36	21.86	107.9	445	.91	.94	.94
38	21.82	105.7	425	.91	.92	.89
40	20.67	100.7	400	.86	.88	.84
42	18.59	92.84	360	.78	.81	.76
44	15.78	83.37	332	.66	.72	.70
46	13.69	75.44	312	.57	.66	.66
48	12.55	70.27	275	.52	.61	.58
50	11.31	64.57	243	.47	.56	.51
52	10.06	58.83	210	.42	.51	.44
54	8.94	54.30	180	.37	.47	.38
56	7.65	49.00	150	.32	.43	.32
58	6.09	41.85	125	.25	.36	.26
60	4.72	34.99	103	.20	.30	.22

Ω = 0.306 atm-cm
δ = 0.161 at 380 nm
0.099 at 500 nm

August 17, 1978 (a.m.)

θ_o	E_c	RB_c	RB_m	Ratio E_c	Ratio RB_c	Ratio RB_m
28	23.99	113.9	660	1	1	1
30	22.90	109.9	615	.95	.96	.93
32	21.69	104.8	590	.90	.92	.89
34	20.39	99.6	565	.85	.87	.86
36	19.06	94.2	530	.79	.83	.80
38	17.72	88.7	510	.74	.78	.77
40	16.33	82.8	475	.68	.73	.72
42	14.99	77.2	442	.62	.68	.67
44	13.79	72.1	415	.57	.63	.63
46	12.85	67.8	385	.54	.60	.58
48	11.46	62.3	352	.48	.55	.53
50	9.41	54.1	321	.39	.47	.49
52	8.25	49.1	291	.34	.43	.44
54	7.49	45.5	260	.31	.40	.39
56			227			.34
58			199			.30
60			175			.27

Ω = 0.323 atm-cm
δ = 0.090 at 380
0.064 at 500

August 17, 1978 (p.m.)

θ_o	E_c	RB_c	RB_m	Ratio E_c	Ratio RB_c	Ratio RB_m
30	24.16	110.7	630	1	1	1
32	21.07	101.1	590	.87	.91	.94
34	19.39	94.6	560	.80	.85	.89
36	16.42	83.9	520	.68	.76	.83
38	15.39	78.2	490	.64	.71	.78
40	13.98	72.7	450	.58	.66	.71
42	13.54	70.2	420	.56	.63	.67
44	12.69	66.7	388	.53	.60	.62
46	10.20	57.4	352	.42	.52	.56
48	9.51	53.9	325	.39	.49	.52
50	8.32	49.0	295	.34	.44	.47
52	7.91	46.5	265	.33	.42	.42
54	6.81	41.6	235	.28	.38	.37
56	5.78	37.0	211	.24	.33	.33
58	4.97	32.9	190	.21	.30	.30
60	4.20	29.0	171	.17	.26	.27

Ω = 0.313 atm-cm

October 12, 1978 (p.m.)

θ_o	E_c	RB_c	RB_m	Ratio E_c	Ratio RB_c	Ratio RB_m
51	10.42	54.8	244	1	1	1
53	9.05	50.3	223	.87	.92	.91
55	7.50	43.1	195	.72	.78	.80
57	6.69	39.8	172	.64	.73	.71
59	5.64	35.6	150	.54	.65	.62
61	4.86	32.5	130	.47	.59	.53
63	3.84	27.3	107	.37	.50	.44
65	3.18	24.0	89	.31	.44	.37
67	2.48	20.3	72	.24	.37	.29
69	1.90	16.9	57.5	.18	.31	.24

Least-square polynomial solution to these data.

$$R_{E_c} = 0.001156\ \theta_o^2 - 0.1834\ \theta_o + 7.338$$

$$R_{RB_c} = 0.0005312\ \theta_o^2 - 0.1017\ \theta_o + 4.804$$

$$R_{RB_m} = 0.0006146\ \theta_o^2 - 0.1169\ \theta_o + 5.375$$

Ω = 0.268 atm-cm
δ = 0.267 at 380 nm
0.204 at 500 nm

October 13, 1978 (p.m.)

θ_o	E_c	RB_c	RB_m	Ratio E_c	Ratio RB_c	Ratio RB_m
53	9.24	50.5	260	1	1	1
55	7.60	45.3	228	.82	.90	.88
57	6.66	41.2	194	.72	.82	.75
59	5.41	35.5	166	.58	.70	.640
61	4.22	29.9	141	.46	.59	.55
63	3.31	25.4	117	.36	.50	.45
65	2.52	21.2	97	.27	.42	.37
67	2.01	17.9	80.5	.22	.35	.31
69	1.54	14.4	65.7	.17	.29	.25

Least-square polynomial solution to these data.

$$R_{E_c} = 0.001849\ \theta_o^2 - 0.2778\ \theta_o + 10.53$$

$$R_{RB_c} = 0.000678\ \theta_o^2 - 0.1284\ \theta_o + 5.911$$

$$R_{RB_m} = 0.001350\ \theta_o^2 - 0.21153\ \theta_o + 8.422$$

$\Omega = 0.293$ atm-cm

Combined Ratios for August 15 and 17, 1978

θ_o	Ratio E_c	Ratio RB_c	Ratio RB_m
34	1	1	1
36	.90	.93	.94
38	.86	.88	.89
40	.79	.83	.83
42	.74	.78	.76
44	.66	.72	.71
46	.58	.65	.66
48	.53	.60	.59
50	.45	.54	.54
52	.41	.50	.48
54	.37	.46	.42
56	.31	.41	.37
58	.26	.36	.32
60	.21	.31	.28

Least-square polynomial solution to these data.

$$R_{E_c} = 0.0002464\ \theta_o^2 - 0.05347\ \theta_o + 2.529$$

$$R_{RB_c} = 0.0001271\ \theta_o^2 - 0.0385\ \theta_o + 2.161$$

$$R_{RB_m} = 0.0001691\ \theta_o^2 - 0.04427\ \theta_o + 2.319$$

$\bar{\Omega} = 0.314$ atm-cm